https://doi.org/10.5194/egusphere-2025-1154
Preprint. Discussion started: 16 April 2025

The Impact of Convection-Permitting Rainfall on the Dryland Water Balance

George Blake[1], Katerina Michaelides[1], Elizabth Kendon[1,2], Mark Cuthbert[3], Michael Bliss Singer[3,4]

[1] School of Geographical Sciences, University of Bristol, Bristol, BS8 BSS, United Kingdom
[2]Met Office Hadley Centre, Fitzroy Road, Exeter, EX1 3PB, United Kingdom
[3]School of Earth and Environmental Sciences, Cardiff University, Cardiff, CF10 3AT, United Kingdom
[4] Earth Research Institute, University of California Santa Barbara, CA 93106, USA

Correspondence to: George Blake (george.blake@bristol.ac.uk)

Abstract. In drylands rainfall is typically delivered during short-lived and localised convective storms, the characteristics of which determine how water is partitioned into different terrestrial stores. However, rainfall datasets used in hydrological modelling and assessments of water resources are typically derived from climate models that are too coarse to represent convective processes that are occurring at scales smaller than the model. In this paper we quantify the impact of climate model representation of convection on the simulated water balance at four locations in the Horn of Africa: a humid site in the Ethiopian Highlands, a semi-arid site in southern Kenya, an arid site in eastern Ethiopia, and a hyper-arid site in northern Somalia. We benchmark the novel pan-Africa convection permitting climate model (CP4A) and its parameterised counterpart (P25) against high-resolution satellite-derived gridded datasets of rainfall (IMERG) and PET (hPET). The comparison shows that explicitly resolving convection improves characterisation of rainfall frequency, intensity, and the relative contribution of low vs high-intensity rainfall to annual totals. We also demonstrate that the representation of convection can impact model PET, although differences in PET between CP4A and P25 are more muted relative to rainfall, and both can capture seasonal and diurnal PET dynamics. To establish how climate model representation of convection can impact hydrology, we then ran a series of one-dimensional hydrological model experiments along an aridity gradient across the Horn of Africa using Hydrus 1-D, where at each of our four sties Hydrus was driven by rainfall and PET from CP4A and P25 (and hPET). We find that the 'drizzle' bias in P25 means when rainfall is propagated through Hydrus, wetting fronts are more restricted to upper soil layers, resulting in higher evaporative losses, lower soil moisture, and bottom drainage in drylands. While at our humid site in the Ethiopian Highlands there are minimal differences in hydrological outcomes, in drylands the more intense and intermittent rainfall in CP4A means surface runoff is up to ten times higher and bottom drainage up to 25 times higher. We conclude that dryland hydrology is highly sensitive to climate model representation of convection, and that forcing hydrological model projections with convectional climate models that parameterise the average effects of convection risks underestimating future crop health, groundwater availability, or flood risk.

https://doi.org/10.5194/egusphere-2025-1154
Preprint. Discussion started: 16 April 2025

1 Introduction

Dryland regions (which for this study refers to any area with an aridity index <= 0.5 rather than 0.65) are characterised by limited and highly variable rainfall, where high temperatures, minimal humidity, and high solar radiation means the atmospheric water demand exceeds the available moisture supply (J Reynolds et al., 2007). When rainfall does occur in drylands, it typically falls during intense, localised, short duration rainstorms that are convective in nature (Nicholson, 2011; Singer and Michaelides, 2017; Singer et al., 2018; Hill et al., 2023). These storms are a critical source of moisture and represent a key control on dryland sub-surface water availability (Singer et al., 2018; Quichimbo et al., 2021, 2023). Therefore, the representation of convection and convective storms in climate models is critical for capturing dryland rainfall characteristics and subsequent water partitioning when propagated through hydrological models. However, the grid resolution of general (global) or regional climate models (GCM/RCMs), which can range from 10 – 250 km, means they are unable to explicitly represent convective processes, which are occurring at the sub-grid scale (Prein et al., 2015; Clark et al., 2016).

The inability of GCM/RCMs to explicitly resolve convection means they may fail to adequately represent dryland rainfall characteristics, which is a potential major limitation in understanding future global climate resilience, as drylands cover ~45% of the Earth's surface, are home to around 3 billion people, and represent the largest biome on Earth (Schimel, 2010; Mirzabaev et al., 2019). For humans living in drylands, their livelihoods are often intrinsically linked to the regional expression of climatic variability, particularly where populations primarily rely on intermittent surface water resources and rainfed pasture and crops (Stringer et al., 2009; Davenport et al., 2017, 2018; Hoffman et al., 2022).

One such region is the Horn of Africa (HOA), where inconsistent seasonal rainfall during their two rainy seasons of Mar – May and Oct – Dec, and increasingly severe and frequent drought (Lyon and DeWitt, 2012; Lyon, 2014; Funk et al; 2019, Wainwright et al; 2019) is increasing the risk of regional food and water insecurity (Cheechi and Robinson, 2013; Nicholson, 2014; Funk et al., 2019). With research suggesting climate change will exacerbate water stress, desertification, and land degradation (Cook et al., 2020; Hoffman et al., 2022; Kimutai et al., 2023), there is a pressing need to understand how future rainfall will translate into surface and subsurface water availability in the HOA.

However, hydrological processes are particularly complex in drylands as the partitioning between infiltration, runoff, evaporation, transpiration, and recharge is highly dependent on the spatial and temporal characteristics of rainfall, rather than annual or seasonal totals (R Taylor et al., 2013; Arpuv et al., 2017; Singer and Michaelides, 2017; Cuthbert et al., 2019; Adloff et al., 2022; Kipkemoi et al., 2021; Quichimbo et al., 2021, 2023). In addition to rainfall characteristics, the dryland water balance is also sensitive how synchronicity between rainfall and evaporative demand impacts antecedent soil moisture conditions (Zhang and Shilling, 2006; Nazarieh et al., 2018; Cuthbert et al., 2019; Schoener and Stone, 2019; Schoener, 2021; Boas and Mallants, 2022), with temporal offsets between potential evapotranspiration (PET) and rainfall capable of directly influencing impacting soil moisture, agricultural yields, and

https://doi.org/10.5194/egusphere-2025-1154
Preprint. Discussion started: 16 April 2025

drought severity (Porporato et al., 2002; Lobell et al., 2011; Vicente-Serrano et al., 2018; Tugwell-Wootton et al., 2020; Kimutai et al., 2023).

The high evaporative demand in drylands means it is typically only high-intensity, short-lived, and localised convective rainfall events that can yield sufficient rainfall for moisture to overcome this PET burden, resulting in high infiltration rates, enhanced soil moisture, and groundwater recharge (R Taylor et al., 2013; Batalha et al., 2018; Kipkemoi et al., 2021; Adloff et al., 2022; Boas and Mallants, 2022). These intense convective events can also yield additional focused recharge when runoff is significant enough to generate flow in dry channels, leading to localised transmission losses (Osborn 1983; Scanlon et al., 2006; Cuthbert et al., 2016, 2019, Singer and Michaelides, 2017; Seddon et al., 2021; Zarate et al 2022; Quichimbo et al., 2021, 2023). Whereas, if rainfall is low-intensity and long-duration, evaporative losses will be higher and rainfall will be quickly returned to the atmosphere (Batalha et al., 2018, Kipkemoi et al., 2021).

The GCMs and RCMs often used to make future assessments of dryland water resources (Crosbie et al., 2010; Mckenna and Sala, 2017; Razack et al., 2019; Cook et al., 2022) poorly represent convection due to their spatial and temporal scale (Prein et al., 2015, Kendon et al., 2017). As climate models with horizontal grid spacings larger than 10 km rely on parameterisation schemes to estimate the average effects of convection occurring at scales smaller than the model scale (Prein et al., 2015). This is a well-known source of model error (Prein et al., 2015; Kendon et al., 2017), which results in 'parameterised' climate models systematically overestimating the frequency of low intensity rainfall events, simulating rainfall too early in the day, and underestimating the magnitude of extreme rainfall (Stephens et al., 2010; Stratton and Stirling, 2012; Prein et al., 2013; Ban et al., 2014; Kendon et al., 2019; Finney et al., 2019). However, computational advances have led to an increase in the availability of convection-permitting model (CPM) simulations, which are run at sufficiently high resolution (< 5 km) to explicitly resolve deep convection and represent a step-change in climate modelling capabilities (Clark et al., 2016). This offers the possibility of assessing whether CPMs can better capture dryland rainfall characteristics, if there are differences in PET dynamics between CPMs and parameterised climate models, and critically is dryland water partitioning sensitive to climate model representation of convection (via its impact on rainfall and PET).

In this study we compare two climate models that use broadly the same model physics but go about representing convection in fundamentally opposing ways. One, a high-resolution (~4.5 km) convection-permitting model explicitly represents convection (CP4A), while the other, a regional climate model (~25 km) parameterises the average effects of convection (P25). While both models simulate comparable annual and seasonal rainfall totals (Kendon et al., 2019; Wainwright et al., 2019), their respective representation of convection is likely to control how rainfall is typically delivered, which could have implications for how moisture propagates through a dryland hydrological system. Furthermore, no studies to date have assessed how model representation of convection can impact the atmospheric variables that control PET. Hence, utilising these two models we consider three key questions:

https://doi.org/10.5194/egusphere-2025-1154
Preprint. Discussion started: 16 April 2025

(1) Does explicitly resolving convection in climate models improve the representation of hydrologically-relevant rainfall metrics in the Horn of Africa?
(2) Does explicitly resolving convection in climate models affect the representation of PET dynamics in the Horn of Africa?
(3) Does the impact of explicitly resolving convection on rainfall and PET influence how water is partitioned between different stores in drylands?

To do this we compare a CPM and a conventional RCM to high-resolution hourly gridded satellite derived datasets of rainfall and PET, focusing on the ability of each model to capture key hydrologically relevant dryland rainfall and PET metrics. Subsequently, we establish how differences in model representation of convection impacts water partitioning when rainfall and PET is propagated through a hydrological model, by running a series of point-based, one-dimensional simulations along an aridity gradient across the HOA.

2 Methods

2.1 Climate Model Description

This study utilises data from two pan-African climate models ran under the Future Climate for Africa (FCFA) Improving Model Processes for African cLimAte (IMPALA) project (Stratton et al 2018; Kendon et al 2019). Both the Convection-Permitting Model for Africa (CP4A) and the 25-km regional model (P25) are configurations of the Met Office Unified Model (Walters et al., 2017). Two ten-year time-slices of hourly data run at a horizontal resolution of 4.5 km x 4.5 km in CP4A and 26 x 39 km in P25 are available for a historical (1997-2007) and a future period (2095-2105 RCP8.5). Both CP4A and P25 utilise the same domain, aerosol and land surface forcing, and are forced by the 25 km Unified Model GCM at their lateral boundaries and Reynolds sea-surface temperature observations (R Reynolds et al., 2007; Walters et al., 2017; Stratton et al., 2018). While CP4A and P25 use different cloud and blended boundary layer schemes, and CP4A also considers moisture conservation, the biggest difference is that the deep convection parameterisation scheme has been 'switched off' in CP4A (Stratton et al., 2018).

However, it is important to note that CP4A uses a uniform soil map that assumes all soils to be sandy, which risks poor representation of soil moisture – precipitation feedbacks that are critical to inducing convective rainfall and a realistic spatial pattern of rainfall in drylands (Taylor et al., 2011, 2012; Hsu et al., 2017; Zhou et al., 2021). There are also clearly limitations with results based upon the use of a single climate model (as opposed to typical practice of employing an ensemble of models), although consistent agreement between CP4A and other CPMs in terms of capturing rainfall characteristics compared to observations increases confidence in CP4A (Kouadio et al., 2018; Luu et al., 2022).

https://doi.org/10.5194/egusphere-2025-1154
Preprint. Discussion started: 16 April 2025

2.2 Climate Data

To establish whether CP4A can better capture dryland rainfall characteristics (relative to P25) we compared both models to the gridded Integrated Multi-satellitE Retrievals for GPM (IMERG, Huffman et al., 2012) rainfall product and an hourly potential evapotranspiration dataset (hPET, Singer et al 2021). IMERG utilises space-based radar, passive microwave, infrared, and rain gauge data from the Global Monthly Precipitation Climatology Centre (Huffman et al., 2012), its high spatial (30 mins) and temporal resolution (half-hourly) means it is the most appropriate for evaluating dryland rainfall metrics (Ageet et al., 2022). However, IMERG is only available from June 2000, so we can only compare CP4A/P25 to 6.5 years of rainfall data.

The hPET global hourly PET dataset (Singer et al., 2021) is derived from the Food and Agriculture Organisations' Penman-Monteith equation for reference crop evapotranspiration (Allen et al., 1998) using the ERA5-Land climate variables (Muñoz Sabater, 2024), it is available at a high spatial (0.1 degrees) and temporal resolution (hourly) and can capture both diurnal and seasonal variability in atmospheric evaporative demand (Singer et al., 2021). To compare against hPET, we computed CP4A and P25 PET with the FAO Penman-Monteith equation using the same seven atmospheric variables that are output from these models:

1. 10 m zonal (u) wind speed (m s-1)
2. 10 m meridional (v) wind speed
3. 2 m dew point temperature (K)
4. 2 m air temperature (K)
5. Surface net solar radiation (J m-2)
6. Surface net thermal radiation (J m-2)
7. Atmospheric surface pressure (Pa)

2.3 Dryland Rainfall Metrics

While other studies have demonstrated that CP4A better captures rainfall frequency, extremes, the diurnal cycle, and the spatial structure of rainfall events (Ban et al., 2014; Prein et al., 2015; Kendon et al., 2017, 2019; Finney et al., 2019, 2020). Here we benchmark CP4A and P25 against a series of metrics that are explicitly indicative of the key dryland rainfall characteristics that control hydrological partitioning:

1. Percentage of annual rainfall delivered via heavy rainfall vs drizzle
2. Maximum dry spell length
3. Extreme rainfall magnitude (99^{th} percentile of rainy season wet hours)

We used the above metrics as dryland hydrology can be more sensitive to the mode of rainfall delivery (light vs intense rainfall) than seasonal/annual totals (R Taylor et al., 2013; Arpuv et al., 2017; Singer and Michaelides, 2017; Cuthbert

https://doi.org/10.5194/egusphere-2025-1154
Preprint. Discussion started: 16 April 2025

et al., 2019; Kipkemoi et al., 2021; Quichimbo et al., 2023), particularly when it comes to extreme rainfall events (R Taylor et al., 2013; Batalha et al., 2018; Adloff et al., 2022; Boas and Mallants, 2022). Furthermore, dry spell length can impact evaporative losses and influence the antecedent soil moisture conditions that can govern the hydrological responses to rainfall (Zhang and Shilling, 2006; Nazarieh et al., 2018; Schoener and Stone, 2019; Schoener, 2021; Boas and Mallants, 2022), with soils typically drying out between convective storms (C Taylor et al., 2011, 2012; Hsu et al., 2017; Zhou et al., 2021).

For the above metrics we define low-intensity rainfall ('drizzle') as any wet hour where rainfall is <= 1 mm/hr, high-intensity ('heavy') rainfall as any wet hour above the 95th percentile (using IMERG) of wet season precipitation, while 'extreme' rainfall is defined as the 99th percentile of wet season precipitation. These percentile-based metrics only consider wet hours (hour >= 0.1 mm of rainfall) during the wettest season (either Jan-Feb, Mar-May, Jun-Sep, and Oct-Dec) for each grid cell across our domain. For dryland regions the wettest season will either be MAM or OND, and for the more humid Ethiopian Highlands it is more likely to be JJAS (Fig.1 & Annex C – Fig. 1C)

To better represent the high-intensity, low-duration nature of rainfall in drylands, our analysis was conducted at hourly rather than three-hourly resolution (Bethou et al., 2019; Kendon et al., 2019; Finney et al., 2019, 2020), as resampling to a coarser timescale dampens the intensity of rainfall and impacts water partitioning (Batalha et al., 2021; Kipkemoi et al., 2021). To ensure consistency, all datasets were re-gridded using first order conservative re-gridding to the P25 grid (26 x 39 km).

2.4 Hydrological Modelling

2.4.1 Hydrus 1-D

We used Hydrus 1-D v4.17 (Šimůnek et al., 2012) to simulate dynamic changes in surface runoff, evaporation, transpiration, soil moisture, and bottom drainage when forced with each climate model rainfall and PET. Hydrus 1-D can simulate water redistribution in the soil subsurface under a wide range of different climatic, soil, and vegetation conditions, and has been widely used to understand soil moisture, evapotranspiration, and groundwater recharge in both arid and humid landscapes (Leterme et al., 2012; McKenna and Sala, 2017; Batalha et al., 2018; Rodriguez et al., 2020; Boas and Mallants, 2022; Corona and Ge, 2022). However, despite its use in dryland settings (McKenna and Sala, 2017, Rodriguez et al., 2020, Boas and Mallants, 2022), it doesn't consider lateral flows, and critically (in a dryland context) it cannot represent 'focused' recharge below streambeds.

Hydrus 1-D was forced with timeseries of rainfall, PET, and Leaf Area Index (LAI) and to analyse how rainfall is partitioned between surface runoff, infiltration, actual evapotranspiration, and drainage below the soil profile (Fig. 2). To simulate the one-dimensional flow of water through saturated, partly saturated, or unsaturated media, the model numerically solves a version of the Richards equation (Richards, 1931; Šimůnek et al., 2012). Thus, it requires parameterisation of soil hydraulic properties, which are typically obtained from in-situ measurements or derived using soil textures filtered through a pedotransfer function (van Genuchten, 1980). It also includes a sink term to account

https://doi.org/10.5194/egusphere-2025-1154
Preprint. Discussion started: 16 April 2025

for root water uptake, which is estimated using the water stress response function detailed by Feddes (1978). For further details on Hydrus 1-D please refer to (Šimůnek et al., 2012).

2.4.2 Hydrological Study Sites

Given the sensitivity of dryland hydrology to rainfall characteristics, we wanted to establish whether relative differences in hydrological outcomes between Hydrus simulations (when forced with CP4A and P25 rainfall/PET) varied with aridity. Hence, we ran four 1-D hydrological simulations along an aridity gradient across the HOA, ranging from humid to hyper-arid (Fig. 1). Aridity values are taken from the CGIAR-CSI (Consortium of International Agricultural Research Centres' Consortium for Spatial Information) (Zomer et al., 2007) using the classification of Mirzabaev et al (2019).

Figure 1 shows the climatic zones of the HOA along with the locations of our four sites, with one site in each of the four major aridity classifications: humid (9.7% of land mass), semi-arid (31.8%), arid (43.6%), and hyper-arid (7.7%). It is worth noting that typically dry sub-humid regions are also classed as dryland, but in this study when we refer to 'drylands', we are conservatively only referring to grid cells with an AI < 0.5. This is due to the limited spatial extent of dry sub-humid areas across the HOA (7.2%). To ensure our one-dimensional hydrological simulations isolate the impact of rainfall characteristics on water partitioning, we aimed to choose locations within each aridity classification where mean annual rainfall and PET was broadly comparable between CP4A and P25. However, at all sites, it is P25 that simulates higher mean annual rainfall (12 – 29% higher) (Table 1) compared to CP4A, this ensures that if fluxes such as soil moisture or bottom drainage are higher when forcing Hydrus with CP4A rainfall, it is reflective of differences in rainfall characteristics rather than simply higher annual totals.

Site	Rainfall **(CP4A)**	PET **(CP4A)**	Vegetation
Site HU (humid) – Ethiopian Highlands	2000 mm (**1730 mm**)	1290 mm (**1400 mm**)	Maize
Site SA (semi-arid) – Southern Kenya	670 mm (**600 mm**)	1620 mm (**1580 mm**)	Shrubs
Site A (arid) – Eastern Ethiopia	430 mm (**350 mm**)	2180 mm (**1920 mm**)	Shrubs
Site HA (hyper-arid) – Northern Somalia	240 mm (**180 mm**)	1970 mm (**1720 mm**)	Bare Soil

Table 1. Mean annual rainfall, PET, and vegetation type at our four study sites. Rainfall and PET simulated by CP4A are in bold. Vegetation type is taken from the iSDAsoil dataset (iSDA, 2024).

https://doi.org/10.5194/egusphere-2025-1154
Preprint. Discussion started: 16 April 2025

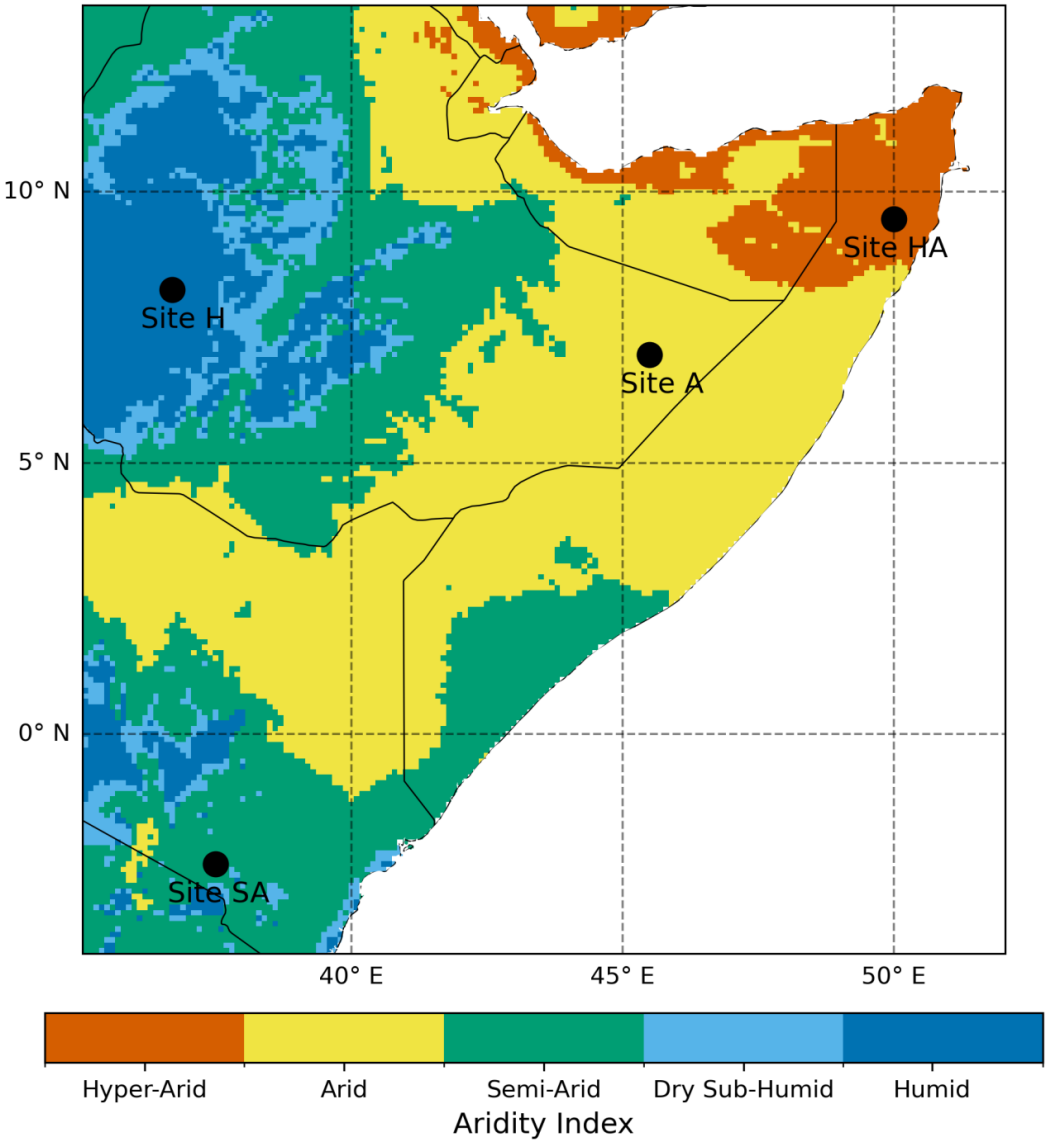

Figure 1. Horn of Africa Aridity Index and Study Site Locations. Location of the four Hydrus locations plotted against aridity index values taken from CGIAR-CSI. Sites are found in the humid Ethiopian Highlands (Site HU), semi-arid southern Kenya (Site SA), arid eastern Ethiopia (Site A), and hyper-arid northern Somalia (Site HA).

2.4.3 Hydrological Model Set Up, Data, and Sensitivity

Our experimental one-dimensional Hydrus simulations examine how climate model representation of convection can control how moisture propagates through a hydrological system, rather than aiming to reproduce 'realistic'

https://doi.org/10.5194/egusphere-2025-1154
Preprint. Discussion started: 16 April 2025

hydrological simulations. However, although our model simulations are experimental, we did use plausible soil hydraulic and vegetation parameters where available.

All Hydrus simulations utilised a three-meter soil profile (preliminary simulations suggested minimal water fluxes below this depth at some locations) with a free draining bottom boundary (no interactions between water Table and soil profile above). For the top boundary layer, we used atmospheric boundary conditions with surface runoff, meaning where model rainfall exceeds the infiltration capacity of the topsoil the water is re-routed as runoff and cannot enter the soil profile (Fig. 2). For all simulations the soil profile was discretized in 2 cm intervals, with a minimum and maximum time step interval of 5 seconds to 20 days (high max time step needed as long periods with no rainfall in drylands). This ensured the model converged (using default Hydrus water content and pressure head tolerances) within 10 timesteps (Hydrus default) and relative mass balance errors remained below 1%. All model runs at each site were initially forced using the mean hourly IMERG and hPET climatology (over 2000-2007) until steady state conditions were reached and relative mass balance errors were below 0.1% (6 – 15 years depending on study site).

Soil hydraulic properties were calculated using Genuchten-Mualem (Van Genuchten, 1980) equations based on soil texture values taken from the iSDAsoil database, which applies a multiscale ensemble machine learning approach to a range of fine-and coarse-scale satellite observations to predict soil properties at 30 m resolution at two depth intervals (0 – 20 cm and 20 – 50 cm) (Hengl et al., 2021). While robust estimates of water movement would require soil textures for the entire profile, here we divided our three-meter profile into two layers following the iSDAsoil data depth intervals: an upper (0 – 20 cm) and lower layer (20 – 300 cm). This approach is a significant simplification as it assumes that soil properties are homogenous at depths below 0.2 m below ground level (mbgl). All simulations were run using the Van-Genuchten-Mualem single porosity model.

To calculate transpiration Hydrus needs land cover (Table 1) and leaf area index (LAI) data, which were taken from iSDA (as of 2019) and the National Centers for Environmental Information AVHRR LAI dataset (Vemote, 2019) respectively. Hydrus uses the Feddes (1978) approach to estimate root water uptake under various pressure heads (water stress) and root densities. For Site HU we utilised Feddes' parameters for maize (from the internal Hydrus database – Wesseling (1991)) and set the maximum rooting depth to 1.2 mbgl (Zinyengere et al., 2011). Shrubs are not included in the internal vegetation database, and there is limited information on Feddes' parameters for dryland shrubs, so we combined data from available literature to estimate a reasonable parameter set (Appendix A - Table B2) (Xia and Shao, 2008; Sela et al., 2015; Watson, 2015). As dryland shrubs tend to be deep-rooted (Stone and Kalisz, 1991; Maeght et al., 2013; Shadwell and February 2017), we assumed they can utilise moisture from the entire soil profile and specified maximum root density at ~0.7 mbgl, which tends to be the depth at which shrub root water uptake is greatest (Geißler et al., 2019).

At Sites SA (southern Kenya) and A (eastern Ethiopia), we ran additional Hydrus simulations using a range of shrub Feddes' parameters (Appendix A - Table B1) as given by Sela et al (2015). Within the range given by Sela et al (2015)

https://doi.org/10.5194/egusphere-2025-1154
Preprint. Discussion started: 16 April 2025

we used the upper parameter set as our 'default' run, as the wilting point corresponded better with other published data (Xia and Shao, 2008, Watson, 2015). At all sites, we also ran Hydrus simulations using low (lowK) and high (highK) hydraulic conductivity soil parameters (Appendix A - Table 1A). Finally, dryland hydrology can also be sensitive to PET as well as rainfall, so we also to assess whether the impact of climate model representation of convection on PET can impact water partitioning, we also forced Hydrus with climate model rainfall but replaced climate model PET with gridded hPET values. Unless stated otherwise, all results refer to simulations forced using climate model rainfall/PET and the default soil hydraulic and Feddes' parameters given in Appendix A Tables 1-2A.

Figure 2. Hydrus Simulations Schematic. Conceptual schematic of how water is partitioned within Hydrus 1D at any given timestep within the simulation. It is important to note that in the above figure both shrubs, maize, and bare soil represented, whereas only one vegetation type can be modelled. Here the schematic is divided to represent the model set up for each site-specific simulation. For all sites the soil profile is divided into two layers (boundary is marked at 20 cm) and is discretised at a resolution of 2 cm. At Site HU, maize roots to a depth of 120 cm, while at Sites SA and A shrubs utilise moisture through the entire 300 cm profile. At Site HA we assume grass cover is extremely sparse, here we only consider bare soil evaporation and no root water uptake (transpiration).

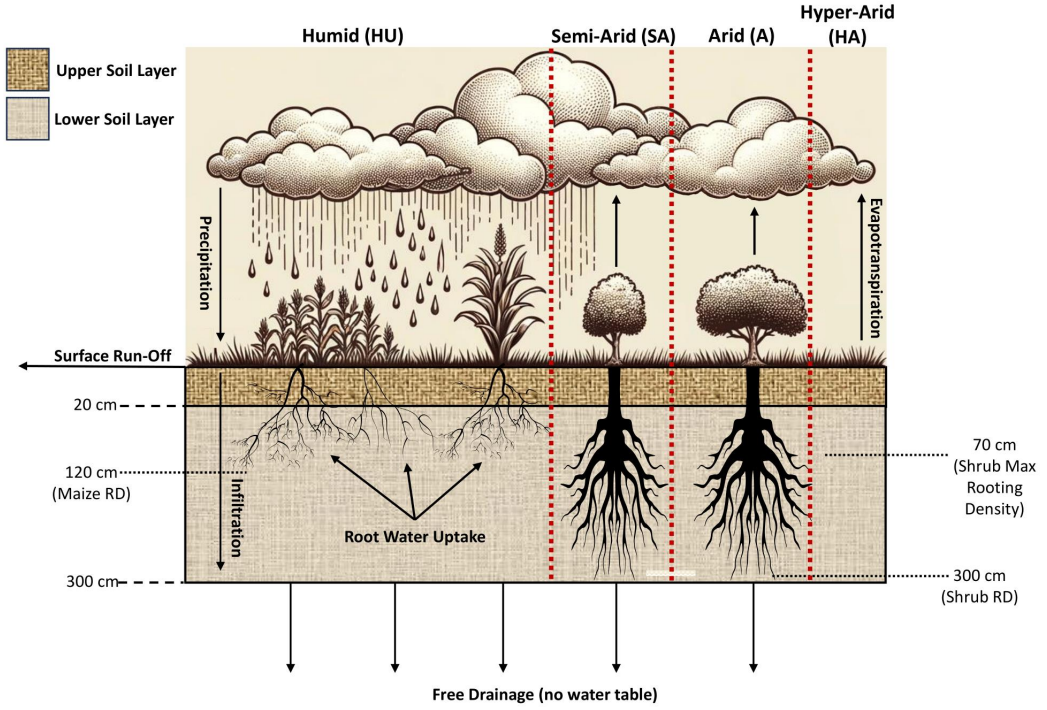

https://doi.org/10.5194/egusphere-2025-1154
Preprint. Discussion started: 16 April 2025

3. Results

3.1 Rainfall

Figures 3(a) and (b) show the distribution of rainfall intensities for all rainfall hours (based on a threshold of 0.1 mm/h) for humid (AI > 0.65) and dryland regions (AI < 0.50) across the HOA. The plots highlight the 'drizzle' effect associated with parameterised climate models (shown by the large frequency peaks in rain hours between 10^{-1} and 10^{1} mm/h), with P25 overestimating the frequency of rainfall events < 1 mm/hr in both regions, but particularly drylands (Fig 3b). CP4A does not simulate the same 'drizzle effect' in drylands and offers a clear improvement in the frequency of dryland rainfall, in both humid and dryland regions CP4A still simulates fewer rainfall events > 10 mm/hr compared to IMERG. Using the Kolmogorov-Smirnov (KS) test shows that while there is still a statistically significant difference in the distribution on rainfall relative to IMERG, the KS statistic is lower (0.03) using CP4A compared to P25 rainfall (0.24).

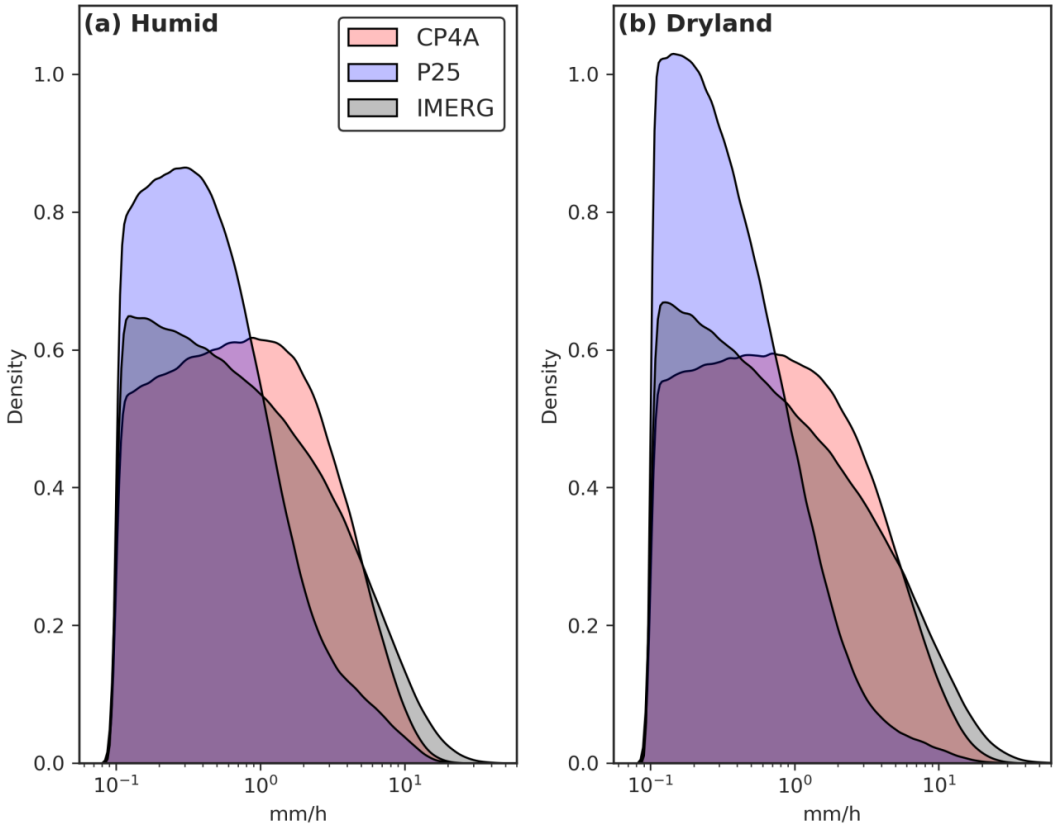

Figure 3. Rainfall KDE Plots. Kernel density estimate (kde) plots of CP4A, P25, and IMERG hourly rainfall in humid (a) (AI >= 0.65) and dryland (b) (AI < 0.5) regions of the Horn of Africa. Plots exclude dry hours by dropping any hours that receive < 0.1 mm/hr.

https://doi.org/10.5194/egusphere-2025-1154
Preprint. Discussion started: 16 April 2025

The tendency for P25 to overestimate the frequency of light rainfall events means most annual rainfall is delivered via events with a magnitude of < 1 mm/hr (Fig. 4a-c) across the HOA. In humid regions, on average P25 simulates 39.0% of annual rainfall falling as 'drizzle' versus 17.1% and 13.6% in CP4A and IMERG respectively. This bias is even more pronounced in dryland areas, where the median proportion of annual rainfall falling as drizzle is 51.5% in P25 versus 14.1% and 13.0% for CP4A and IMERG. Apart from a few isolated locations, no areas in the drylands receive more than 20% of rainfall via 'drizzle' in CP4A and IMERG.

This frequent 'drizzle' in P25 also results in an underestimation of maximum dry spell length (CDD – consecutive dry days) compared to IMERG and CP4A (Fig. 4d - f). While both climate models replicate the spatial pattern of CDD observed in IMERG (CDD is higher in drylands), the relative biases of P25/CP4A compared to IMERG are opposing.

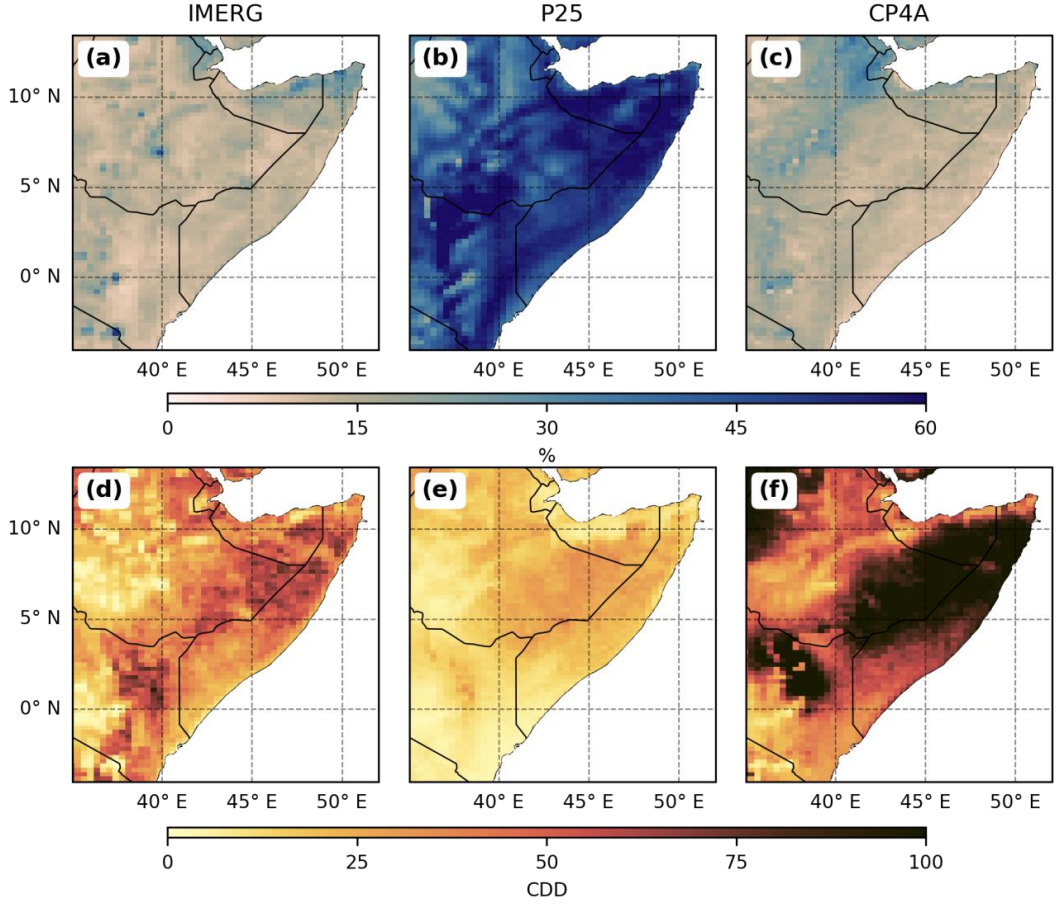

Figure 4. Percentage of Annual Rainfall delivered as drizzle and maximum number of consecutive dry days. Percentage of mean annual rainfall that falls as 'drizzle', where 'drizzle' is any rain hour with an intensity <= 1 mm/hr (top panel) for IMERG (a), P25 (b), and CP4A (c). Bottom Panel - Mean annual maximum dry spell length, where a dry hour is any hour that receives less than 0.1 mm of rain IMERG (a), P25 (b), and CP4A (c).

https://doi.org/10.5194/egusphere-2025-1154
Preprint. Discussion started: 16 April 2025

In drylands, the median longest dry spell in P25 is ~18 days, with an inter-quartile range (IQR) of 11 – 24 days. Even in arid (AI < 0.2) regions median CDD only increased to ~20 days (IQR 13 – 26 days). Whereas in CP4A there are dry spells of over 100 days across large parts of eastern Ethiopia, northern Somalia, and northern Kenya, and the CDD IQR for drylands is 48 – 95 days and 61 – 102 in arid regions. In other words, relative to IMERG, P25 underestimates CDD and CP4A overestimates CDD. In IMERG, median dry spell length in drylands is ~38 days with an IQR 27 – 51 days, which increases to 35 – 55 days in arid regions. The tendency for CP4A to overestimate CDD remains in humid regions, where the median max CDD is ~38 days (IQR 24 – 73 days) versus ~10days (7 – 14 days) and ~13 days (IQR 7 – 19 days) for P25 and IMERG respectively.

Figures 5a–c compares the 'extreme' rainfall (99th percentile of wet hours in the wettest rainy season) and shows both climate models underestimate the magnitude of extremes relative to IMERG in humid and dryland regions. However, the bias is reduced in CP4A, which in line with other studies using three-hourly data (Bethou et al., 2019; Kendon et al., 2019; Finney et al., 2019, 2020). The improvement when using CP4A is more pronounced in drylands, where the median (IQR) hourly 99th percentile values are 15.0 mm (12.4 – 16.3 mm) (IMERG), 12.5 mm (CP4A) (10.9 – 14.4 mm), and 5.8 mm (4.6 – 7.1 mm) (P25). Differences between CP4A and P25 are more muted in humid regions, where the median value is just 36% higher in CP4A vs P25 (vs > 110% in drylands), and IQR ranges overlap (CP4A: 8.4 – 11.1 mm and P25: 5.4 – 9.2 mm). Also, unlike CP4A, P25 simulates higher 99th percentiles in humid rather than dryland regions (7.1 mm vs 5.8 mm), although this may be related to the use of wet rather than all hours when computing percentiles, as P25 dramatically overestimates the frequency of rainfall (most notably in drylands).

Explicitly resolving convection also means a greater proportion of annual rainfall is delivered via 'heavy' rainfall events in CP4A relative to P25 (Fig. 5d– f), most notably in drylands. Figures 5d –f shows the percentage of annual rainfall that falls as 'heavy' rainfall, however, rather than using a consistent mm/hr intensity across the entire domain, we use the 95th percentile of IMERG rainfall as our threshold for 'heavy' rainfall (Appendix B – Figure 1B). This means our threshold varies grid cell by grid cell (2.3 mm – 10.9 mm in humid regions and 2.9 mm – 16.2 mm in dryland regions) and ensures we reflect the tendency for a greater percentage of rainfall to fall as 'heavy' events in drylands (Fig. 5d). Given we have used the IMERG 95th percentile as our threshold, we are more focused on comparing CP4A and P25 to each other rather than IMERG.

In western humid regions both CP4A and P25 simulate comparable contributions from 'heavy' rainfall, with overlapping IQRs of 8.8% - 18.3% (CP4A) and 5.1% - 13.4% (P25). Whereas in drylands to the east, the IQR of the percentage of annual rainfall falling during 'heavy' events is 13.5% - 25.4% in CP4A versus 3.8% - 11.0% in P25. This difference becomes more pronounced in the arid regions of eastern Ethiopia and Somalia where the median values are 21.5% and 7.8% respectively. CP4A also better replicates the spatial pattern observed in IMERG, where dryland regions in the east tend to receive more rainfall via 'heavy' events relative to humid regions in the west (median values of 19.2% vs 13.8%), whereas the opposite is true in P25 (median values of 6.8% vs 8.4%).

https://doi.org/10.5194/egusphere-2025-1154
Preprint. Discussion started: 16 April 2025

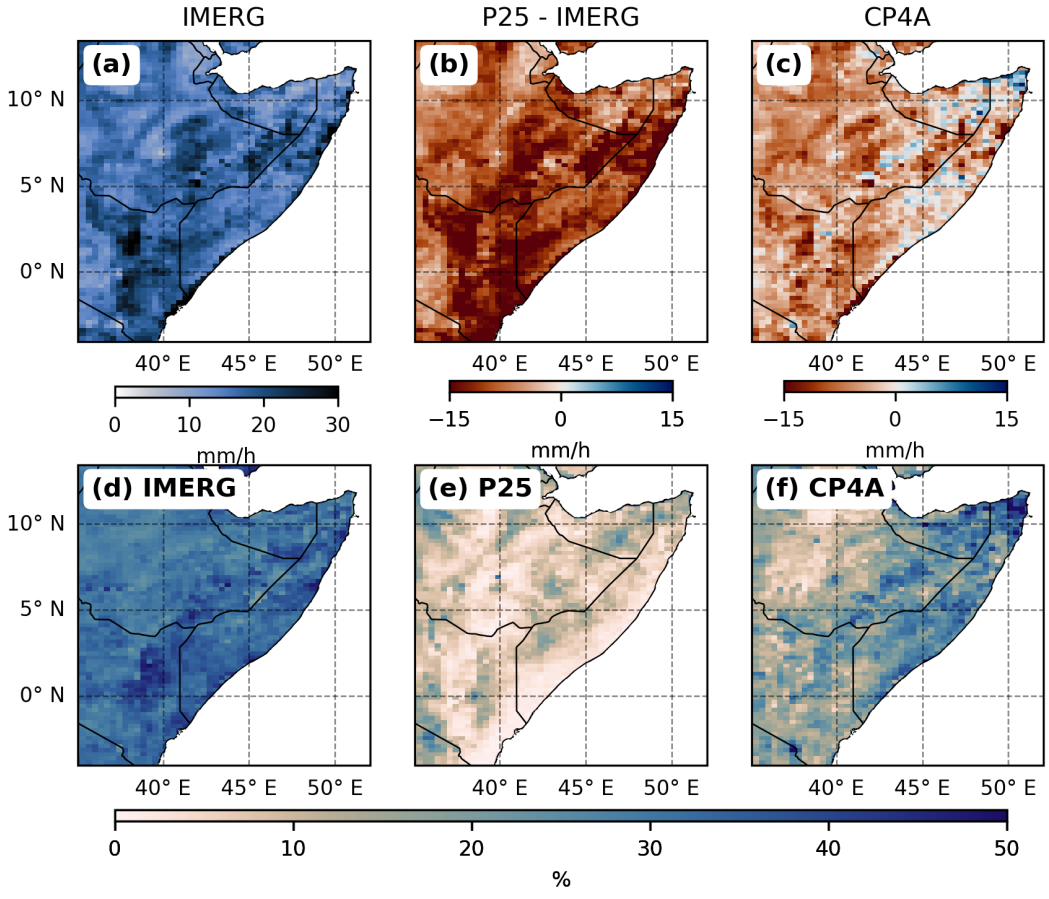

Figure 5. 99th Percentiles and percentage of rainfall delivered via 'heavy' events. Wet season 'extreme' precipitation (top panel) for IMERG observations (a), and differences with respect to IMERG for P25 (b) and CP4A (c). Extreme precipitation is defined as the 99th percentile of all wet hours, where wet hours are any hours that receive >= 0.1 mm of rain. Bottom Panel - Percentage of mean annual rainfall that falls during 'heavy' rainfall events, in this context we are defining a 'heavy' rainfall event as the 95th percentile of IMERG rainfall (wet hours).

3.2 Potential Evapotranspiration (PET)

Calculating PET with climate model atmospheric variables replicates the spatial pattern of PET given by hPET, with higher evaporative demand across the drylands in the east compared to the more humid Ethiopian Highlands (Fig. 6a–c), and generally provide reasonable annual PET magnitudes across the region (hPET – 1715 mm, CP4A – 1787 mm, P25 – 1883 mm). CP4A simulates marginally higher mean annual PET (relative to P25) in humid regions (1416 mm vs 1387 mm), while the opposite is true in arid regions (1901 mm vs 2027 mm). The most pronounced difference in PET simulations between CP4A and P25 is the arid regions of Somalia and Eastern Ethiopia. Across any grid cells

https://doi.org/10.5194/egusphere-2025-1154
Preprint. Discussion started: 16 April 2025

classified as arid, CP4A simulates PET that exceeds 2000 mm a^{-1} in just 18% of cells, versus 53% and 43% in P25 and hPET, respectively.

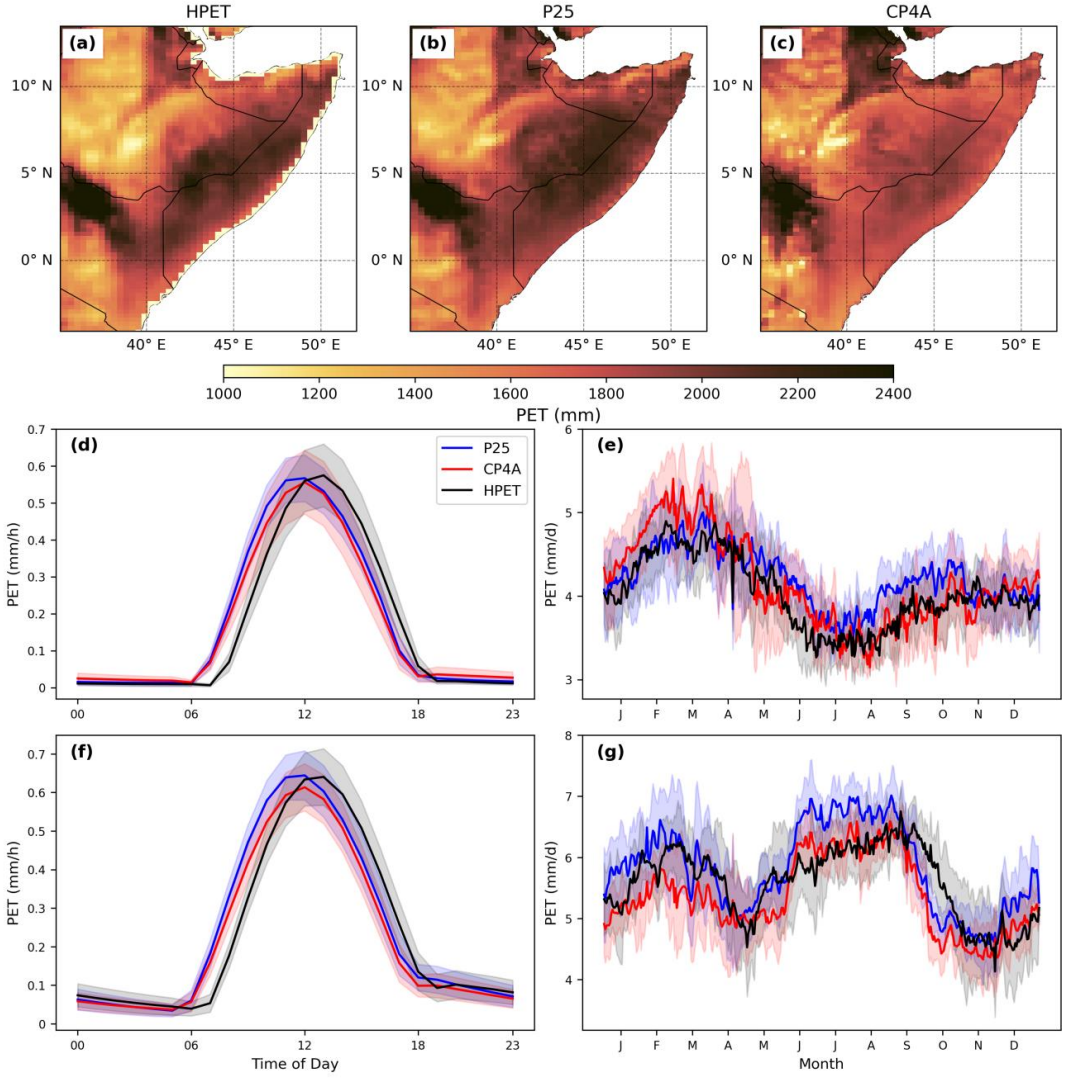

Figure 6. Mean annual PET, diurnal PET cycle, and daily climatology of PET. Spatial plots of mean annual PET (top panel) for HPET observations (a), P25 (b), and CP4A (c). Mean diurnal cycle and daily climatology of PET in humid (AI > 0.65) (middle panel) and arid to hyper-arid (AI <= 0.2) (bottom panel) regions of the Horn of Africa for HPET, P25, and CP4A.

Both climate models also simulate a clear diurnal cycle (Fig. 6d-f) and replicate the hPET seasonal cycle (Fig. 6e-g) in both humid and arid regions, although, both models simulate earlier peaks in diurnal PET compared to hPET (12:00 vs 13:00). In arid regions P25 tends to simulate higher PET during the dry seasons of Jan-Feb and Jun-Sep relative to both CP4A and hPET (Fig. 6g), the IQR ranges (medians) for each dataset in arid regions during dry seasons (JF &

https://doi.org/10.5194/egusphere-2025-1154
Preprint. Discussion started: 16 April 2025

JJAS) are as follows: hPET: 919 mm – 1135 mm (1035 mm), CP4A: 908 mm – 1086 mm (1000 mm), P25 is 978 mm – 1185 mm (1098 mm). During the rainy seasons (MAM & OND) P25 also simulates higher PET (905 mm) in arid regions relative to CP4A (860 mm) but lower PET compared to hPET (912 mm).

Multi-linear regression (MLR) shows differences in temperature and dew point temperature explain most PET variability in humid and dryland regions in both climate models (Appendix B - Table B1). Although in dryland regions meridional wind speed also exerts a significant effect on PET (Appendix B - Table B1), with higher wind speeds in P25 during JJAS appearing to be partly driving the higher P25 PET during JJAS (Appendix B – Figure 2B).

3.3 Water Partitioning

At each hydrological study site, CP4A and P25 correctly simulate the seasonal cycle of rainfall and tend to produce broadly comparable seasonal totals (Appendix C - Figure 1C), although on average P25 delivers higher annual rainfall (Table 2). Both models also produce comparable seasonal PET totals and simulate the same seasonal cycle, although P25 simulates substantially higher PET during JJAS at Site HA (Appendix C – Figure 2C), following the results discussed in section 3.2. Critically, the differences in rainfall characteristics follow the results discussed above in section 3.1, meaning at each site CP4A tends to deliver more rainfall via infrequent and intense events, while P25 delivers rainfall via near-continuous drizzle. A full breakdown of the metrics discussed above (CDD, 99th percentiles, % of rainfall delivered via ‘drizzle’ vs ‘heavy’ events) for each site is given below in Table 2.

	Site HU	Site SA	Site A	Site HA
P25 Total Rainfall (mm)	2000	670	430	240
CP4A Total Rainfall (mm)	1730	600	350	180
P25 Total 'Drizzle' (mm) **(% of Annual Total)**	650 **(33%)**	358 **(53%)**	234 **(54%)**	133 **(55%)**
CP4A Total 'Drizzle' (mm) **(% of Annual Total)**	329 **(19%)**	80 **(13%)**	40 **(11%)**	22 **(12%)**
P25 Total 'Heavy' Rain (mm) **(% of Annual Total)**	449 **(22%)**	75 **(11%)**	53 **(12%)**	71 **(30%)**
CP4A Total ‘Heavy' Rain (mm) **(% of Annual Total)**	378 **(22%)**	149 **(25%)**	170 **(49%)**	148 **(82%)**
P25 99th Percentile (mm/h)	8.5	5.8	5.5	4.3
CP4A 99th Percentile (mm/h)	9.1	15.6	11.2	17.9
P25 Max CDD (days)	13	12	8	20
CP4A Max CDD (days)	41	43	105	107

Table 2. Mean annual rainfall, ‘drizzle’, ‘heavy” rain, 99th wet season percentiles, and maximum number of consecutive dry days (CDD) at each of our four sites. The percentage of annual rainfall that falls as ‘drizzle’ or ‘heavy’ rain (based on the 95th percentile of wet season IMERG rainfall) is given in brackets.

From our Hydrus 1-D simulations we analysed soil moisture, surface runoff, evaporation, transpiration, and bottom drainage. Fig. 7a-d show histograms of depth-integrated θs (% soil saturation in entire 300 cm of the soil profile) at each site, where despite simulating lower total rainfall, forcing Hydrus with CP4A rainfall results in higher θs at dryland locations. While there is statistically significant difference in medians (Mann-Whitney) and distributions

https://doi.org/10.5194/egusphere-2025-1154
Preprint. Discussion started: 16 April 2025

(Kolmogorov-Smirnov) at all sites, the differences are more pronounced in drylands (KS statistics: HU– 0.08, SA – 0.29, A – 0.37, HA – 0.92). Within the three-meter profile, the IQR of θs using CP4A (P25) is 42.7% - 59.0% (35.4% - 45.1%), 29.74% - 33.7% (27.0% - 30.8%), 47.8% - 49.5% (40.5% - 41.1%), 60.6% - 77.7% (59.6% - 79.4%) at sites SA, A, HA, and HU, respectively (differences at site A are more pronounced if we consider depth-integrated θs at 1.2 mbgl, as below this depth there are minimal fluxes) (Appendix C – Table C1).

At all depths (20 - 40 cm intervals) and at every location there are statistically significant differences in θ_s between CP4A and P25 for both medians and distributions, with differences in the KS statistic generally increasing with depth (Appendix C - Table C3). Depth-integrated θs masks differences in median θs relative to taking median θs at specific depths. For example, the relative difference in θs between driving Hydrus with CP4A (vs P25) at Site SA increases from + 7.5% at a depth of 90 cm, to 16.1% at 2.1 mbgl, while at Site HA the difference ranges from 17.0% (0.2 mbgl) to 23.1% (1.2 mbgl).

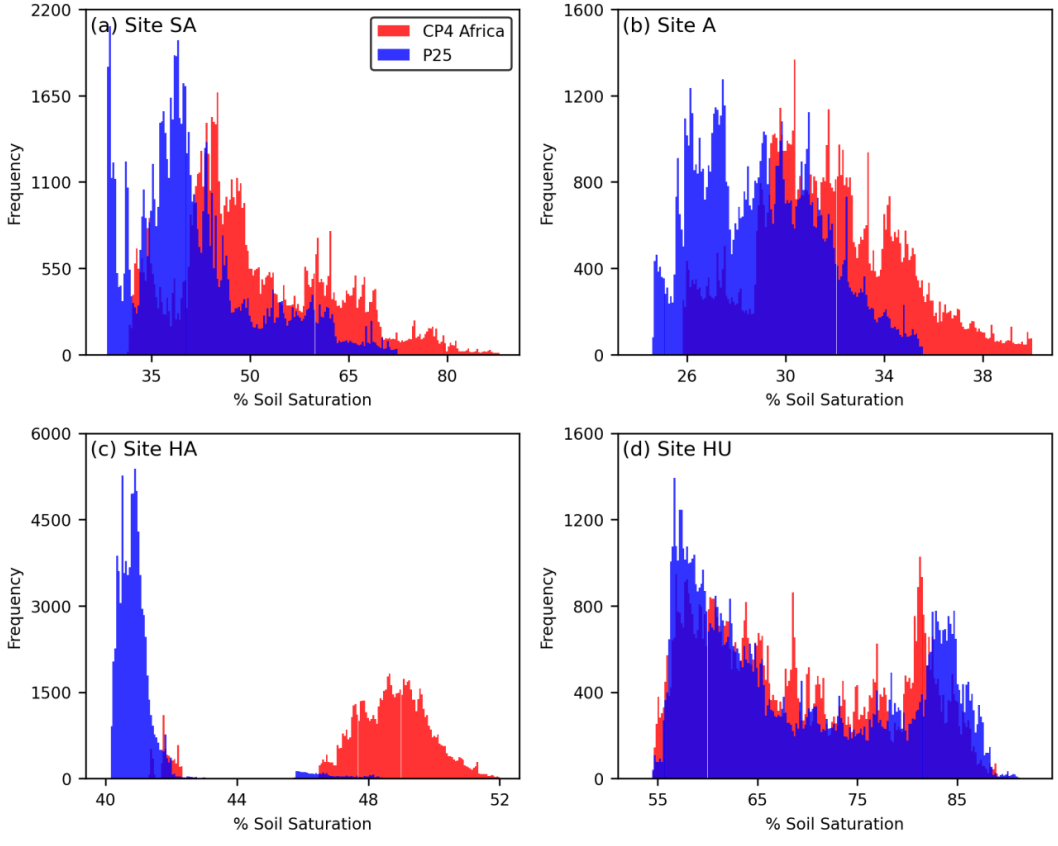

Figure 7. Depth Integrated Soil Moisture Distributions. Modelled distribution of depth integrated soil moisture in the three-meter soil profile when driving Hydrus using P25 (blue) and CP4A (red) rainfall and PET at our semi-arid (a), arid (b), hyper-arid (c), and humid locations (d).

https://doi.org/10.5194/egusphere-2025-1154
Preprint. Discussion started: 16 April 2025

The finding that driving Hydrus with CP4A rainfall and PET yields higher soil moisture remains consistent regardless of the soil hydraulic parameters used (Appendix C - Table C2), or for Sites SA and A where shrubs are the dominant vegetations, regardless of the Feddes' parameters used (Appendix C – Table C4).

Figures 8a-h visualises the deeper wetting fronts in drylands when forcing Hydrus with CP4A, most notably at Sites SA and HA. These differences in wetting front depth could have implications when using CP4A or P25 to model crop or vegetation health modelling. For example, while differences in median depth integrated θs at Site A is less than three percentage points, shallower wetting fronts means θs is above the wilting point (WP) (for shrubs) at a depth of 1.2 mbgl for 0-44% of the Hydrus simulation when forced using P25 (depending on whether you use the upper or lower WP threshold – see Appendix A Table A2), but the range is 1-83% using CP4A (Fig. 8b). It is a similar story at Site SA, where θs is above WP for 27-100% of the time using P25, versus 50-100% using CP4A (Fig. 8a).

These results also highlight the need to accurately quantify the Feddes' parameters used for any given vegetation, as varying the threshold used to define the WP based on the shrub Feddes' parameters given by Sela et al (2015) (Appendix A – Table A2) can reduce the time at which θs is above the WP at Site SA from 83% to 1% for CP4A and 44% to 0% for P25 respectively. But the key finding is that regardless of the Feddes' parameters used, θs is either above the wilting point for longer when forcing Hydrus with CP4A, or where both models simulate θs as always above the WP, using CP4A means θs is high enough for vegetation to transpire at the maximum rate for longer (Site SA – 78% vs 57%, Site A – 13% vs 0%).

To establish whether higher soil moisture in Hydrus CP4A sims were a function of differences in rainfall characteristics or simply lower PET in CP4A at each site, we also forced Hydrus with climate model rainfall and hPET (rather than model PET). Once again, at all depths and at every site, there are statistically significant differences in θs between Hydrus simulations when forced with CP4A/P25 rainfall and hPET, although KS statistics are marginally lower (Appendix C – Table 5C). However, PET alone can exert an influence; the percentage of time θs is above the WP at Site SA is lower when forcing Hydrus with CP4A rainfall and hPET (41% vs 50%), although θs is still above these thresholds for longer using CP4A (41% vs 24%). The reduction is especially pronounced when considering the WP at Site A, where the percentage of time θs is above the WP (using the lower WP threshold) drops from 83/44% to 44/21% for CP4A and P25 respectively when running Hydrus with hPET.

https://doi.org/10.5194/egusphere-2025-1154
Preprint. Discussion started: 16 April 2025

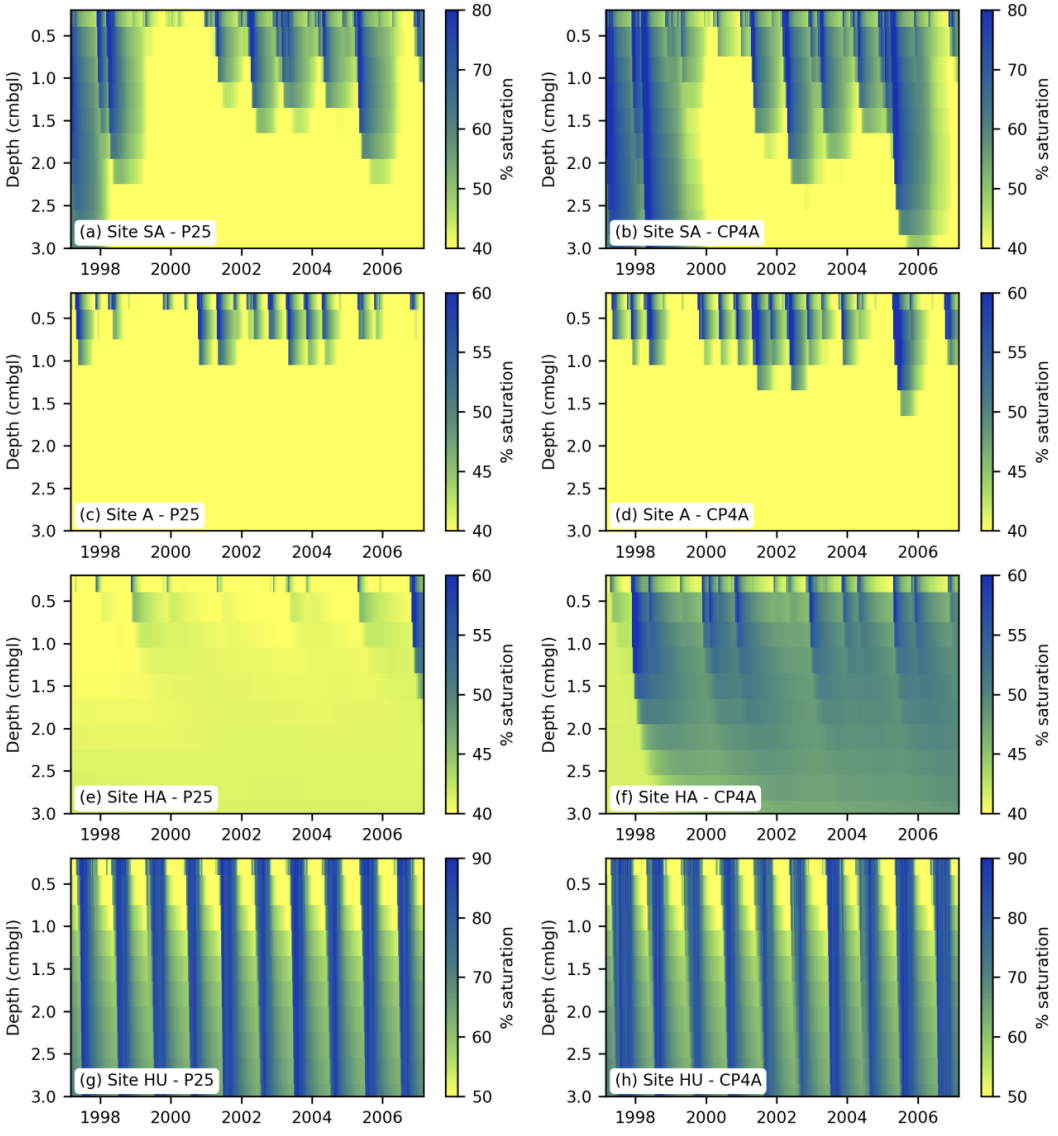

Figure 8. Modelled soil moisture profiles using P25 (left) and CP4A (right) rainfall and PET to drive Hydrus at our semi-arid (a-b), arid (c-d), hyper-arid (e-f), and humid (g-h) locations across the HOA.

Figure 10 details how water is partitioned between surface runoff, evaporation, transpiration, and bottom drainage when CP4A/P25 rainfall and PET is propagated through Hydrus (also see Appendix C – Table 6C). Given θs tends to be above the WP for longer in the CP4A runs, and shrubs can transpire at the maximum rate for longer, it is unsurprising that Figs. 10a - f shows substantially higher transpiration at Sites SA (2392 mm vs 1724 mm) & A (893 mm vs 694) when using CP4A rainfall. The difference in the relative percentage of infiltration lost to transpiration is

https://doi.org/10.5194/egusphere-2025-1154
Preprint. Discussion started: 16 April 2025

even more pronounced, as P25 simulates higher total rainfall and lower surface runoff (Fig. 10a). Higher transpiration totals in drylands are due to the shallower wetting fronts using P25 rainfall resulting in higher evaporative losses, at SA & A 79%-83% of infiltration is returned to the atmosphere when Hydrus is forced with P25, versus 67% – 72% using CP4A rainfall. At Site HA the respective values are 92% vs 98%, while at Site HU evaporative losses are near identical (23.3% vs 23.6%), and transpiration is higher in the P25 Hydrus simulations (Appendix C – Table 6C).

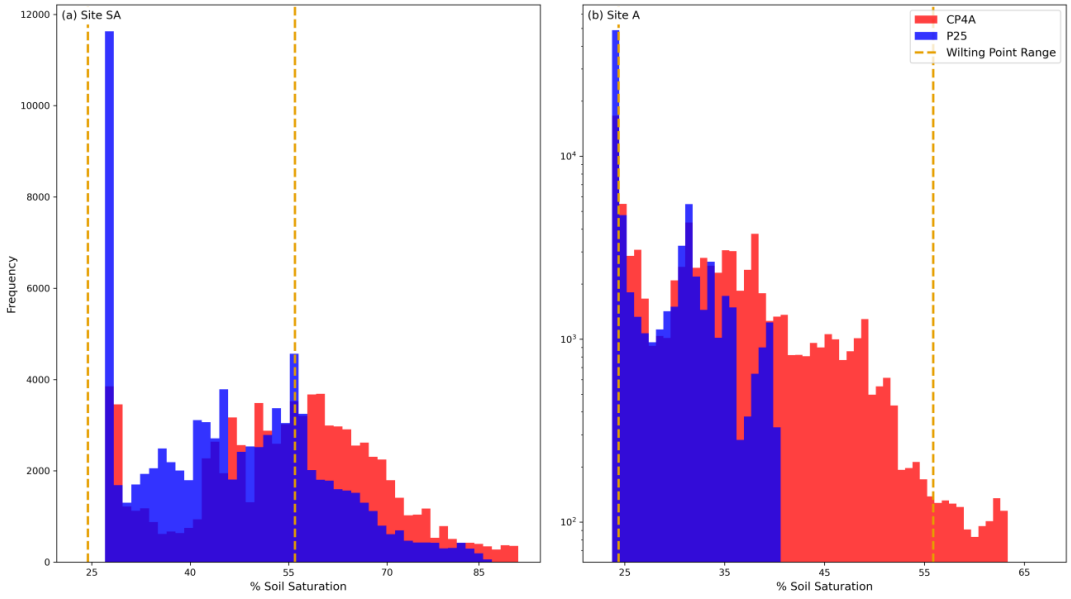

Figure 9. Soil Moisture Distributions with Wilting Points. Modelled distribution of soil moisture at 1.2 mbgl at Site SA (a) and A (b) using P25 (blue) and CP4A (red) rainfall and PET. Green dashed line (a) marks the θs threshold at which shrub roots can no longer extract water at the maximum rate, red dashed line (b) marks the wilting point.

Higher evaporative losses when forcing Hydrus with P25 rainfall are not solely related to higher climate model PET using P25, it remains consistent even when forcing Hydrus with hPET (rather than model PET) (Appendix C – Table 7C). Counterintuitively, in the CP4A runs, using hPET increases evaporative losses by 4%-9% across the four sites despite mean annual lower PET being lower (temporal offsets in rainfall and evaporative demand can impact hydrological fluxes). However, while enhanced evaporative losses in CP4A Hydrus runs forced with hPET reduces transpiration totals, they remain significantly higher than P25 runs in drylands (30%-36% higher in absolute terms) (Appendix C – Table 7C). Transpiration totals are also sensitive to the Feddes' parameters used, but it does impact the relative bias in totals between the CP4A and P25 Hydrus runs (Appendix C – Table 8C).

https://doi.org/10.5194/egusphere-2025-1154
Preprint. Discussion started: 16 April 2025

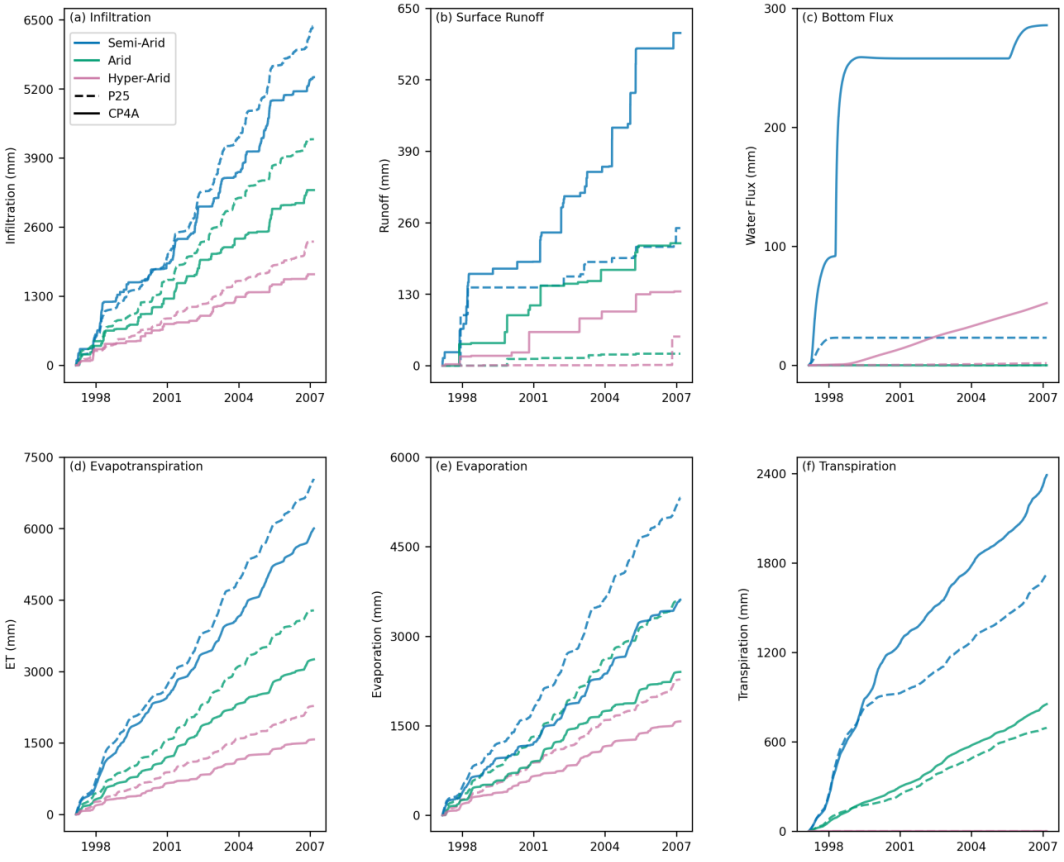

Figure 10. Cumulative Rainfall, PET, Runoff, Evaporation, Transpiration, and Deep Infiltration. Modelled components of the water balance using CP4A (solid lines) and P25 (dashed lines) rainfall/PET as input for Hydrus 1-D. Plots show the infiltration (a), surface run-off (b), bottom drainage (c), evapotranspiration (d), evaporation (e), and transpiration (f) at our semi-arid, arid, and hyper-arid locations.

Despite lower total rainfall at our dryland sites, surface runoff is greater when using CP4A rainfall, over twice as high as P25 at Sites SA and HA (605 mm vs 250 mm & 135 vs 53 mm), and up to ten times higher at Site A (223 mm vs 22 mm). In dryland locations, between 6% and 10% of rainfall is lost to runoff when Hydrus is forced with CP4A rainfall versus 0.3 - 2% with P25 rainfall. There are also large differences in bottom drainage from the soil profile, however it is important to note that this metric is not indicative of groundwater recharge, as in reality it is unlikely the water table would be so shallow, and moisture could still be lost to transpiration through deep rooted shrubs (Stone and Kalisz, 1991; Maeght et al., 2013; Shadwell and February 2017). Driving Hydrus with CP4A rainfall produces higher bottom drainage at dryland sites despite receiving less rainfall overall; 283 vs 23 mm at Site SA and 52 vs 2 mm at Site HA (there was no drainage at Site A. At our humid location (Site HU) P25 simulated 21% higher bottom drainage, closely following the difference in the volume of cumulative rainfall delivered (15%).

https://doi.org/10.5194/egusphere-2025-1154
Preprint. Discussion started: 16 April 2025

4. Discussion

In this paper we evaluated how climate model representation of convection influences its representation of rainfall and PET characteristics across the Horn of Africa (HOA), and what impact this has on the 1D water balance at four sites along an aridity gradient in the HOA. In line with other studies, we find that convection-permitting climate models (CPMs) perform better than parameterised climate models (those that parameterise the average effects of convection) when compared against satellite-derived rainfall observations (in terms of capturing key dryland rainfall metrics). So while both CP4A and P25 simulate comparable annual/seasonal totals, they deliver their rainfall in fundamentally opposing manners (light/frequent vs heavy/infrequent), resulting in differing hydrological outcomes when their output is propagated through a hydrological model. This study also verifies that while dryland hydrology is more sensitive to PET than humid regions, differing hydrological outcomes are primarily driven by rainfall characteristics, and climate model representation of convection exerts a greater control on rainfall over PET.

The ability of CPMs to better represent rainfall frequency, intensity, and the magnitude of extremes is well documented (Prein et al., 2015, Kouadio et al., 2018; Berthou et al., 2019; Luu et al., 2022), including in the context of the HOA (Bethou et al., 2019; Kendon et al., 2019; Finney et al., 2019; 2020). This study demonstrates this improvement is most marked in dryland regions of the HOA (AI <= 0.5) compared to more humid (AI > 0.65) regions (Ethiopian Highlands). This is problematic, as despite their reduced skill in drylands, conventional climate models (those that parameterise the average effects of convection) are widely used to make future projections of dryland rainfall (Huang et al., 2017) and used as driving datasets for hydrological modelling (Crosbie et al., 2010; Mckenna and Sala, 2017; Razack et al., 2019; Cook et al., 2022).

Our modelling demonstrates water partitioning in drylands is sensitive to the magnitude-duration spectrum of rainfall delivery (R Taylor et al., 2013; Arpuv et al., 2017; Singer and Michaelides, 2017; Cuthbert et al., 2019; Kipkemoi et al., 2021; Adloff et al., 2022, Quichimbo et al., 2023). That two climate model products based on the same global model configuration (Walters et al., 2017), with comparable annual totals, and seasonal cycles (Wainwright et al., 2021) produce such differing hydrological outcomes when propagated through a simple 1-D model highlights the importance of carefully selecting driving datasets in hydrological studies. The importance of this choice increases with aridity, as while in humid regions forcing Hydrus with CP4A or P25 has minimal impact on the 1D water balance, in drylands using CP4A increases average soil moisture, and results in markedly higher surface runoff, transpiration, and bottom drainage. Although even in humid regions, studies have found differences in hydrological outcomes between CPMs and parameterised climate models, such as increased surface runoff (Folwell et al., 2022) and higher flood risk when forcing hydrological models with CPM rainfall (Ascott et al., 2023; Archer et al., 2024). And while no flood risk assessments using CP4A have been conducted across the HOA at time of writing, it is reasonable to assume that greater sub-daily rainfall extremes (Bethou et al., 2019; Kendon et al., 2019; Finney et al., 2019, 2020) and surface runoff will result in greater flood hazard potential in the HOA when forcing hydrological models with CPM rainfall.

https://doi.org/10.5194/egusphere-2025-1154
Preprint. Discussion started: 16 April 2025

This highlights a key risk with the continuing use of parameterised climate models in dryland hydrological studies, as they could yield unrepresentative hydrological fluxes that could have implications for societies and livelihoods. For example, while most hydrological studies tend not to distinguish between soil evaporation and transpiration and only report evapotranspiration, our results show moisture lost to evaporation is far higher when forcing Hydrus with P25, while using CP4A increases the volume of water available for transpiration within the root zone, meaning transpiration is higher and continues longer into the dry season (Folwell et al., 2022). This discrepancy is likely related to both rainfall magnitude and how rainfall frequency influences antecedent moisture conditions near the surface. Either way, our work shows that even where ET is comparable, forcing crop yield/suitability models using parameterised climate model rainfall could risk underestimating crop yields and overestimating the risk of failure, or incorrectly suggesting regions may become unsuitable for staple crops (particularly for deeper-rooted crops). In dryland regions of sub-Saharan Africa, where livelihoods are heavily dependent on subsistence agriculture and pasture (Davenport et al., 2017, 2018; Hoffman et al., 2022), incorporating CPM rainfall into agricultural impact assessments could provide more realistic projections of future change.

Furthermore, our results showing enhanced drainage from the bottom of the soil profile when forcing Hydrus with CP4A (despite lower seasonal rainfall) supports other research showing the magnitude of groundwater recharge in drylands does not linearly trend with higher seasonal rainfall totals. Groundwater recharge is sensitive to rainfall characteristics, particularly rainfall intensity, where if rainfall is of sufficient intensity it can generate overland flow, channelized streamflow, and transmission losses in ephemeral rivers (R Taylor et al., 2013; Batalha et al., 2018; Boas and Mallants, 2022). For example, in the context of the HOA, despite a decline in seasonal rainfall totals, groundwater storage is increasing (Adloff et al., 2022). However, this decline in seasonal rainfall has been driven by a later onset and earlier cessation of the MAM ('long') rains season rather than any reduction in rainfall intensity (Wainwright et al., 2019), with positive trends in extreme rainfall appearing to sustain groundwater storage across the region (Adloff et al., 2022). These observed relationships and our hydrological simulations undermine the relevance of making detailed future projections of water resources using conventional climate models that cannot explicitly resolve convective processes and struggle to capture observed rainfall characteristics.

However, while improved representation of rainfall characteristics and atmospheric dynamics in CPMs increases our confidence in future projections of changes in rainfall characteristics (Bethou et al., 2019; Kendon et al., 2019; Finney et al., 2019, 2020), CPMs are not currently a panacea for the wider uncertainty that limits our understanding of future climate change impacts in the HOA. As while explicitly resolving convection can influence regional circulation patterns (Finney et al., 2020), it is unlikely CPMs will resolve the failure of climate models to reproduce the observed drying trend in MAM (long rains) rainfall over the last 30 years (Lyon and Vigaud, 2017; Wainwright et al., 2019; Schwarzwald and Seager, 2024) and their inability to capture important modes of variability and wider large-scale processes (Schwarzwald et al., 2023). As while data is limited, future projections show CP4A follows CMIP models in continuing to project higher rainfall across the HOA (including during the long rains) (Kendon et al., 2019; Wainwright et al., 2021).

https://doi.org/10.5194/egusphere-2025-1154
Preprint. Discussion started: 16 April 2025

Given this uncertainty and the computational costs associated with CPM simulations, utilising stochastic rainfall generators (Singer et al., 2018; Rios Gaona et al., 2024) and process-based scaling approaches consistent with CPM model behaviour can be used to produce time-evolving projections to explore a range of plausible futures in the HOA (Klein et al., 2021). Taking a 'storyline' approach (add reference) built around stochastic scenarios could provide more valuable insights that simply forcing hydrological simulations using RCMs or GCMs that struggle to capture the mean climate state as well as the nature of dryland rainfall, as this risks producing misrepresentative projections of metrics such soil moisture, transpiration, and groundwater recharge, which could contribute to sub-optimal decision making around long-term land use or water supply policy.

5. Conclusions

In this study we find that explicitly resolving convection improves the ability of climate models to capture the nature of dryland rainfall relative to those that parameterise the average effects of convection. Using CP4A dramatically reduces the systemic 'drizzle' bias seen in P25 and better captures dry spell length, the magnitude of extremes, and the contribution of heavy rainfall events to seasonal totals. This means that, despite using similar model physics and simulating comparable seasonal totals, climate model representation of convection can translate into different hydrological outcomes when rainfall is propagated through a simple one-dimensional model. In dryland locations, although simulating lower total rainfall and infiltration, driving Hydrus 1-D with CP4A rainfall produces higher soil moisture, transpiration, and bottom drainage. As although total infiltration is higher when using P25, the 'drizzle' bias means this infiltration is restricted to the upper layers of the soil profile and is quickly returned to the atmosphere as evaporation. Our results also show that while PET can influence hydrological outcomes, dryland hydrology is more sensitive to the impact of climate model representation of convection on rainfall. Any assessments of dryland hydrological resources must carefully consider the driving datasets utilised, particularly in future projections, where the use of parameterised climate model as a driving dataset could result in misrepresentative projections of societally relevant outcomes of the hydrologic cycle relative to more physically robust CPM simulations.

6. Appendices

6.1 Appendix A

Appendix A details the parameters that were altered between the different Hydrus simulations used at each site. Table A1 lists the soil parameters used for our three simulation categories: lowK, def, and highK. Where def (**given in bold**) refers to default soil parameters that are used for all simulations discussed in the main text, lowK refers to low hydraulic conductivity simulations, and highK is high hydraulic conductivity simulations. For example, at Site A hydraulic conductivity (K_s) ranges from 3.5 mm/h to 21.8 mm/h.

These soil parameters were estimated using Genuchten-Mualem (Van Genuchten, 1980) equations based on soil texture values taken from the Innovate Solutions for Decision Agriculture (iSDA) soil database (Hengl et al., 2021).

https://doi.org/10.5194/egusphere-2025-1154
Preprint. Discussion started: 16 April 2025

Where *Qr* refers to residual soil water content, *Qs* is the saturated water content, *Alpha* is Parameter *a* in the soil water retention function [L^{-1}], *n* is parameter *n* in the soil water retention function, K_s is the saturated hydraulic conductivity [LT^{-1}], and *I* is the tortuosity parameter in the conductivity function [-]. Differences in parameters between the lowK and highK simulations were based on taking the lower and upper sand percentage given in the iSDA soil database (Hengl et al., 2021).

Site H (Humid)							
Scenario	Depth	*Qr*	*Qs*	*Alpha*	*n*	*Ks (mm/h)*	*I*
lowK	0 - 20 cm	0.103	0.545	0.002	1.339	18.342	0.500
lowK	20 - 500 cm	0.105	0.543	0.002	1.315	15.650	0.500
def	**0 - 20 cm**	**0.096**	**0.525**	**0.002**	**1.384**	**19.117**	**0.500**
def	**20 - 500 cm**	**0.100**	**0.529**	**0.002**	**1.349**	**17.833**	**0.500**
highK	0 - 20 cm	0.084	0.510	0.002	1.405	22.588	0.500
highK	20 - 500 cm	0.090	0.512	0.002	1.384	19.996	0.500
Site SA (Semi-Arid)							
Scenario	Depth	*Qr*	*Qs*	*Alpha*	*n*	*Ks (mm/h)*	*I*
lowK	0 - 20 cm	0.076	0.416	0.001	1.405	3.221	0.500
lowK	20 - 500 cm	0.081	0.423	0.002	1.351	3.204	0.500
def	**0 - 20 cm**	**0.068**	**0.409**	**0.002**	**1.400**	**5.658**	**0.500**
def	**20 - 500 cm**	**0.076**	**0.418**	**0.002**	**1.354**	**4.175**	**0.500**
highK	0 - 20 cm	0.066	0.408	0.002	1.401	6.663	0.500
highK	20 - 500 cm	0.072	0.417	0.002	1.367	6.100	0.500
Site A (Arid)							
Scenario	Depth	*Qr*	*Qs*	*Alpha*	*n*	*Ks (mm/h)*	*I*
lowK	0 - 20 cm	0.081	0.431	0.001	1.426	3.542	0.500
lowK	20 - 500 cm	0.085	0.436	0.001	1.404	3.338	0.500
def	**0 - 20 cm**	**0.067**	**0.418**	**0.002**	**1.415**	**7.558**	**0.500**
def	**20 - 500 cm**	**0.069**	**0.419**	**0.002**	**1.404**	**6.363**	**0.500**
highK	0 - 20 cm	0.055	0.414	0.003	1.475	21.817	0.500
highK	20 - 500 cm	0.058	0.413	0.002	1.439	16.004	0.500
Site HA (Hyper-Arid)							
Scenario	Depth	*Qr*	*Qs*	*Alpha*	*n*	*Ks (mm/h)*	*I*
lowK	0 - 20 cm	0.070	0.417	0.002	1.400	5.779	0.500
lowK	20 - 500 cm	0.069	0.417	0.002	1.394	6.783	0.500
def	**0 - 20 cm**	**0.067**	**0.417**	**0.002**	**1.406**	**7.633**	**0.500**
def	**20 - 500 cm**	**0.069**	**0.417**	**0.002**	**1.394**	**6.783**	**0.500**
highK	0 - 20 cm	0.056	0.413	0.003	1.480	21.646	0.500
highK	20 - 500 cm	0.056	0.411	0.003	1.466	19.329	0.500

Table A1 - Soil Hydraulic parameters used in all Hydrus simulation at our humid (HU), semi-arid (SA), arid (A), and hyper-arid (HA) sites across the HOA.

Table A2 shows the Feddes' parameters used to compute root water uptake (transpiration) within Hydrus (Feddes, 1978). Where *P0* is pressure value at which roots start to extract water from the soil, *POpt* is the pressure head at which roots extract water at the maximum possible rate, *P2H* is the pressure head at which roots can no longer

https://doi.org/10.5194/egusphere-2025-1154
Preprint. Discussion started: 16 April 2025

extract water at the maximum possible rate (assumes a potential transpiration rate of *r2H*), *P2L* is the same above but instead assumes a maximum possible transpiration rate of *r2L*, and *P3* is the value of the pressure head at which roots can no uptake any water from the soil (wilting point). Vegetation type was taken from iSDA based on 2019 data (iSDA, 2024).

Hydrus has an internal database of Feddes' parameters for various crop types, the maize parameters were taken from this database and are based on Wesseling (1991). However, shrubs are not in this database and there is very little published information on Feddes' parameters for shrubs. We were able to locate some thresholds for dryland shrubs: *Acacia Mearsii*, *Caragana korshinkii*, and *Sarcopoterium spinosum* (Xia and Shao, 2008, Sela et al., 2015, Watson, 2015). Sela et al (2015) provided a range of Feddes' parameters used in their calibration process to correctly quantify transpiration rates of *Caragana korshinkii* in Hydrus 1-D, settling on an optimal parameter set. However, we decided to use the upper range (here referred to as def) of the parameters given by Sela et al (2015) as they better matched estimates given by Xia and Shoa (2008) and Watson (2015), particularly the wilting point. However, to ensure results were consistent regardless of the Feddes' parameters chosen, we also using the optimal and lower values provided by Sela et al (2015). However, unless stated otherwise all results reported in the main body of text were computed using the upper (def) Feddes' values – **given in bold below.**

Feddes' Parameter	*P0*	*POpt*	*P2H*	*P2L*	*P3*	*r2H (mm/h)*	*r2L (mm/h)*
Shrubs Upper (def)	**-150**	**-300**	**-5000**	**-15000**	**-240000**	**0.208**	**0.042**
Shrubs Mid	-58	-224	-326	-6700	-15570	0.208	0.042
Shrubs Lower	0	-150	-300	-5000	-15000	0.208	0.042
Maize	-150	-300	-3250	-6000	-80000	0.208	0.042

Table A2 – Feddes parameters controlling root water uptake for shrubs and maize used in Hydrus 1-D simulations. Values were for shrubs were taken from Sela et al (2015) and maize from Wesseling (1991).

6.2 Appendix B

Appendix B provides additional figures and materials on the analyses of CP4A/P25 rainfall and PET simulations (sections 3.1 and 3.2). Figure 1B shows the magnitude of the 95th percentile of IMERG wet season rainfall (wet hours only). These values were used as the threshold to define want rainfall intensity can be deemed 'heavy' within Fig. 5a-c in the main body of text. In humid regions the intensity ranges from 2 to 11 mm/h (mean of 7.7 mm/h), and in arid regions it ranges from 3 to 16 mm/h (mean of 8.5 mm/h).

Table B1 shows the results of a multi-linear regression between the daily PET climatology and the daily climatology of the seven atmospheric variables used to compute PET in humid and arid regions of the Horn of Africa. These results are discussed in the main body of text under section 3.2.

https://doi.org/10.5194/egusphere-2025-1154
Preprint. Discussion started: 16 April 2025

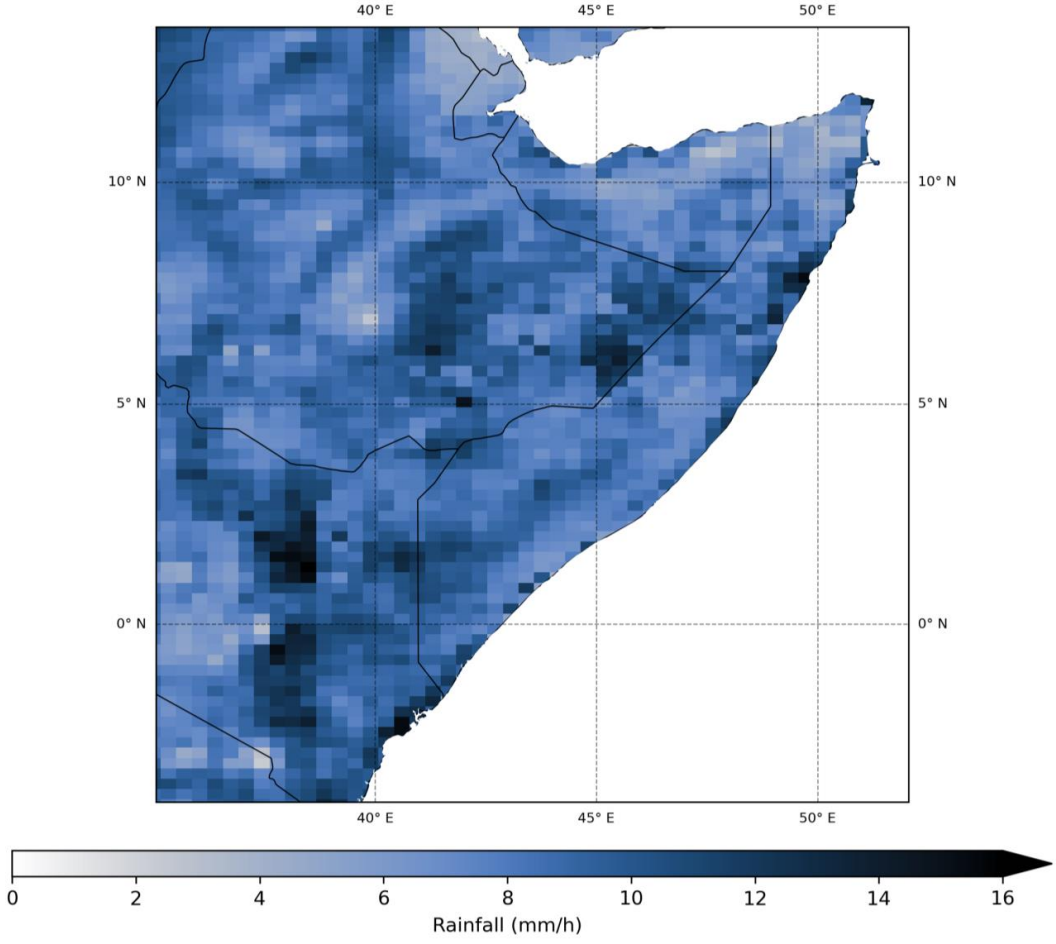

Figure B1 - 95th percentile of IMERG wet season precipitation. Calculated using wet hours, where any wet hours are any hour that receives >= 0.1 mm of rainfall.

Humid Regions					
Variable	Coefficient	Std Error	P>|t|	0.025 CI	0.975 CI
Temp	0.127 (**0.438**)	0.028 (**0.046**)	0 (**0.000**)	0.072 (**0.349**)	0.182 (**0.529**)
Dew Point	0.152 (**-0.129**)	0.021 (**0.031**)	0 (**0.000**)	0.112 (**-0.191**)	0.193 (**-0.068**)
Surface Pressure	0.0001 (**-0.002**)	0.000 (**0.000**)	0.58 (**0.000**)	0.000 (**-0.002**)	0.000 (**-0.001**)
Short Wave Radiation	7.2e-7 (**7.9e-07**)	1.6e-7 (**2.2e-7**)	0.000 (**0.001**)	4.1e-7 (**3.4e-7**)	1.0e-6 (**1.2e-6**)
Long Wave Radiation	-7.9e-6 (**2.6e-6**)	1.4e-6 (**1.8e-6**)	0.000 (**0.149**)	-1.1E-5 (**-9.5e-7**)	-5.1E-6 (**6.2e-6**)
Meridional Wind	0.041 (**-0.108**)	0.024 (**0.034**)	0.081 (**0.002**)	-0.005 (**-0.174**)	0.088 (**-0.041**)

https://doi.org/10.5194/egusphere-2025-1154
Preprint. Discussion started: 16 April 2025

Zonal Wind	-0.181 (**-0.178**)	0.027 (**0.039**)	0 (**0.000**)	-0.235 (**-0.255**)	-0.127 (**-0.100**)
Arid Regions					
Variable	Coefficient	Std Error	P>|t|	0.025 CI	0.975 CI
Temp	0.285 (**0.232**)	0.033 (**0.027**)	0.000 (**0.000**)	0.220 (**0.179**)	0.349 (**0.285**)
Dew Point	-0.364 (**-0.391**)	0.026 (**0.018**)	0.000 (**0.000**)	-0.401 (**-0.426**)	-0.327 (**-0.356**)
Surface Pressure	0.0009 (**-0.001**)	0.000 (**0.000**)	0.58 (**0.000**)	-0.001 (**-0.001**)	-0.001 (**-0.000**)
Short Wave Radiation	2.0e-06 (**7.0e-6**)	2.1e-07 (**4.5e-7**)	0.000 (**0.001**)	1.6e-06 (**6.1e-06**)	2.4e-06 (**7.8e-06**)
Long Wave Radiation	9.6e-06 (**1.2e-5**)	1.4e-06 (**1.2e-6**)	0.000 (**0.149**)	6.8e-06 (**1.0e-5**)	1.2e-05 (**1.5e-5**)
Meridional Wind	0.178 (**0.103**)	0.025 (**0.019**)	0.000 (**0.002**)	0.130 (**0.066**)	0.226 (**0.139**)
Zonal Wind	-0.095 (**0.016**)	0.026 (**0.019**)	0.000 (**0.000**)	-0.146 (**-0.022**)	-0.044 (**0.053**)

Table B1 - Results of the multi-linear regression analysis on the drivers of PET in CP4A and P25 in humid (AI > 0.65) and arid (AI <= 0.2) regions of the HOA. Bold values refer to CP4A, while non-bold values refer to P25.

Figure B2 shows the daily meridional wind speed climatology in arid regions of the Horn of Africa. It appears that the positive significant relationship between meridional wind speed and PET (Table B1) is the driving factor behind higher PET in P25 during the months of June to September (see Fig. 3g)

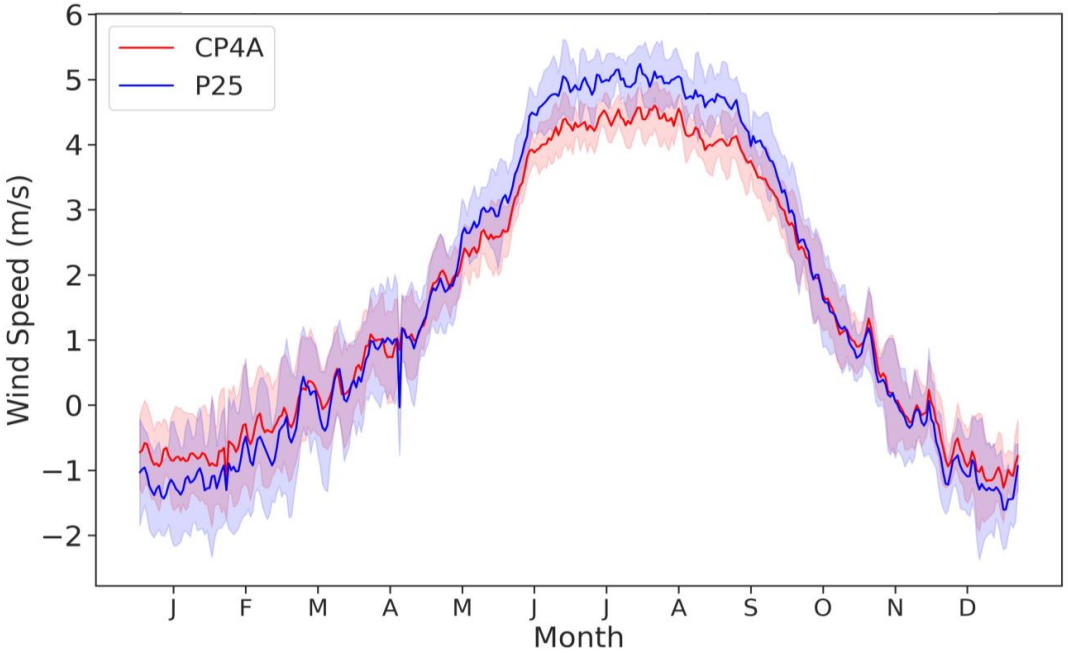

Figure B2 - Daily climatology of meridional wind speed in arid (AI < 0.2) regions of the HOA.

https://doi.org/10.5194/egusphere-2025-1154
Preprint. Discussion started: 16 April 2025

6.3 Appendix C

Appendix C provides additional figures and tables relevant to the analysis of Hydrus simulations (section 3.3). Figure C1 shows the mean monthly CP4A and P25 rainfall at each of our four sites. Both models broadly capture the observed seasonality in the region (Wainwright et al., 2019), simulating the bimodal rainfall regime at our dryland sites (Sites SA, A, and HA) and the unimodal regime in the humid Ethiopian Highlands (Site HU). However, it is worth noting that P25 tends to simulate rainfall in every month (including July and August) at our dryland sites (CP4A simulates negligible rainfall) and simulates substantially higher rainfall totals during June and July at Site HU.

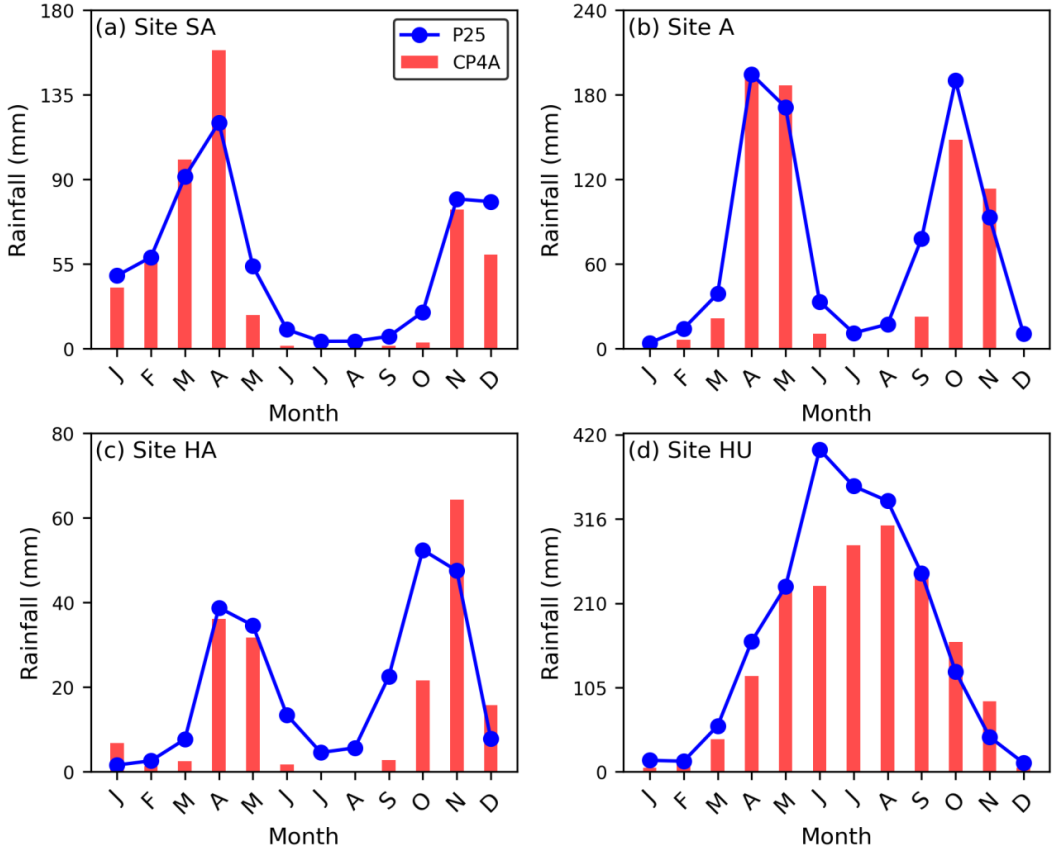

Figure C1 – Mean monthly rainfall at each of our four hydrological study sites.

Figure C2 shows mean monthly CP4A and P25 PET at each of our four study sites. At all sites both models simulate comparable seasonal cycles and totals, although P25 consistently simulates higher PET at Sites A and HA. It is also worth noting that P25 simulates substantially higher PET during the months June – August, matching the higher JJAS PET simulated by P25 across the entire arid region of the HOA.

https://doi.org/10.5194/egusphere-2025-1154
Preprint. Discussion started: 16 April 2025

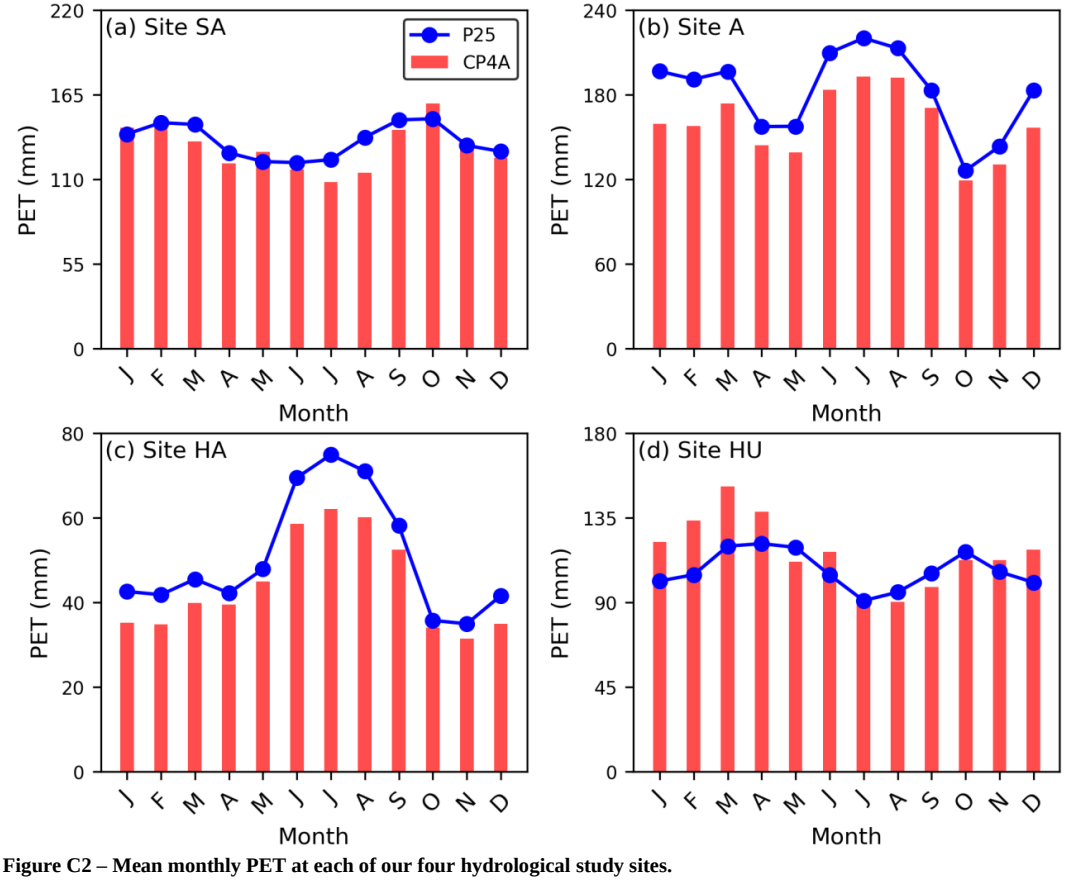

Figure C2 – Mean monthly PET at each of our four hydrological study sites.

Figure C3 shows the raw time series of rainfall at each study site, it provides a clear demonstration of the tendency for CP4A to simulate heavier rainfall events, as well as more frequent intense rainfall events at our dryland study sites (Sites SA, A, and HA). Whereas at our humid site in the Ethiopian Highlands, the differences are far more muted and at times it is P25 that is simulating heavier rainfall events.

https://doi.org/10.5194/egusphere-2025-1154
Preprint. Discussion started: 16 April 2025

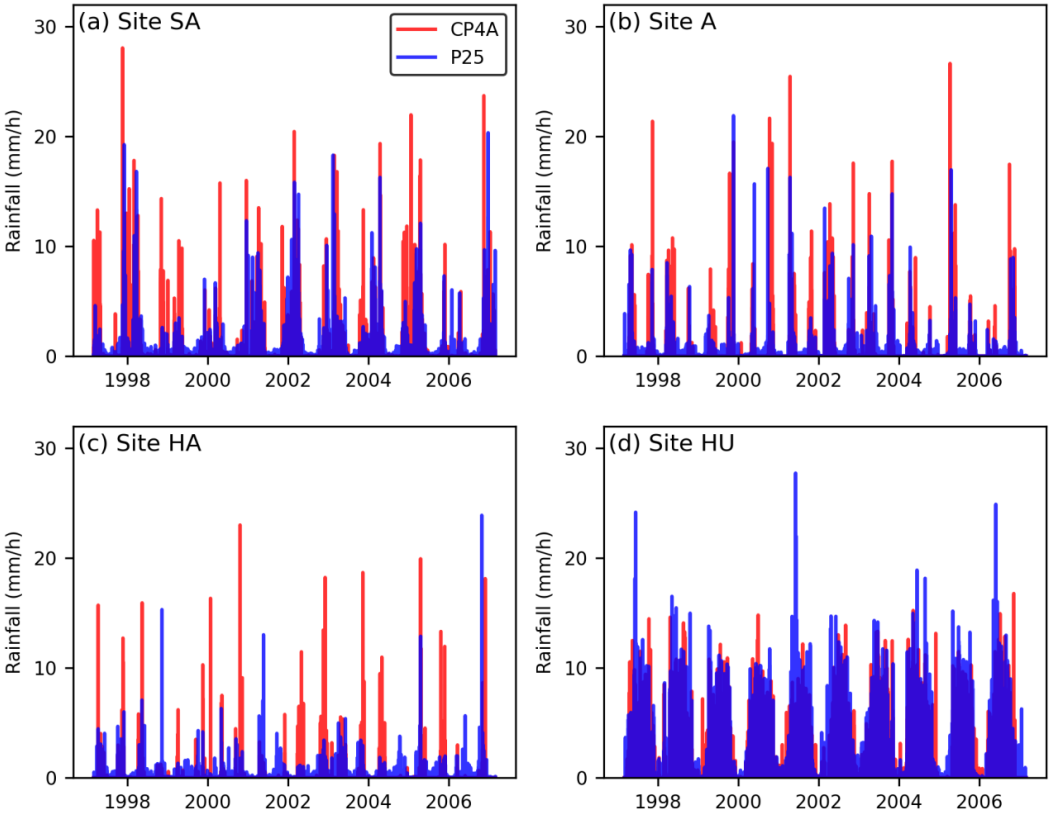

Figure C3 – Raw time series of rainfall at each of our four hydrological study sites.

Table C1 shows the interquartile ranges (IQRs) of soil moisture in the upper 1.2 meters of the soil profile and the entire three-meter profile at each study site.

1.2 Meters Below Ground Level	**Site SA**	**Site A**	**Site HA**	**Site HU**
CP4A	49.7 - 63.6	37.7 - 46.5	47.2 - 51.3	53.0 - 78.9
P25	43.4 - 58.2	31.4 - 41.0	39.7 - 41.1	51.6 - 81.3
3.0 Meters Below Ground Level				
CP4A	42.7 - 59.0	29.7 - 33.7	47.8 - 49.5	60.6 - 77.7
P25	35.4 - 45.1	27.0 - 30.8	40.5 - 41.1	59.6 - 79.4

Table C1 – Interquartile ranges of depth integrated soil moisture in the upper 1.2 meters of the soil profile, and the entire three-meter profile. All values refer to the % saturation.

While the IQR does overlap at each site between the Hydrus simulations driven by CP4A and P25, soil moisture is always higher when Hydrus is forced by CP4A rainfall. This is supported by Table C2, which shows the relative percentage difference in median soil moisture between CP4A and P25, with CP4A simulating 10-20% higher median soil moisture at our dryland sites in the default Hydrus runs.

https://doi.org/10.5194/egusphere-2025-1154
Preprint. Discussion started: 16 April 2025

Hydrus Run (depth - meters below ground level)	Site SA	Site A	Site HA	Site HU
Low Hydraulic Conductivity (1.2 mbgl)	10.6	10.5	17.0	5.2
Low Hydraulic Conductivity (3.0 mbgl)	14.4	5.1	14.7	2.5
Default (1.2 mbgl)	**10.3**	**15.5**	**21.4**	**2.5**
Default (3.0 mbgl)	**20.7**	**9.1**	**19.4**	**5.2**
High Hydraulic Conductivity (1.2 mbgl)	10.4	32.0	22.3	5.7
High Hydraulic Conductivity (3.0 mbgl)	22.6	21.9	25.5	2.6

Table C2 – Relative percentage difference in median depth integrated soil moisture between CP4A and P25 Hydrus runs. Default (given in bold) refers to default soil parameters that are used for all simulations discussed in the main text, lowK refers to low hydraulic conductivity simulations, and highK is high hydraulic conductivity simulations. See Appendix 6.1 for more details on each simulation. For all values reported, it is a positive percentage difference between CP4A and P25 soil moisture. Eg CP4A simulates higher soil moisture in all cases.

This tendency for differences between CP4A and P25 Hydrus runs to be higher in drylands is also supported by Table C3, which shows that differences in soil moisture distributions are more pronounced (based on the Kolmogorov-Smirnov statistic) at the dryland sites versus Site HU.

Depth (meters below ground level)	Site SA	Site A	Site HA	Site HU
0.2 mbgl	0.16	0.14	0.74	0.07
0.6 mbgl	0.22	0.27	0.89	0.07
0.9 mbgl	0.22	0.44	0.93	0.08
1.2 mbgl	0.23	0.40	0.94	0.08
1.5 mbgl	0.35	0.49	0.98	0.08
1.8 mbgl	0.46	0.15	0.99	0.09
2.1 mbgl	0.41	0.00	1.00	0.09
2.4 mbgl	0.49	0.00	1.00	0.09
2.7 mbgl	0.38	0.00	1.00	0.09
3.0 mbgl	0.38	0.00	0.85	0.08

Table C3 - Kolmogorov–Smirnov (KS) test statistics comparing soil moisture distributions at our hydrological four sites across different depths. Higher KS values indicate greater differences between distributions. All results are statistically significant ($p < 0.05$). Site HA consistently shows the largest differences, while Site HU exhibits the smallest KS values, suggesting the least divergence. All results refer to Hydrus simulations driven by CP4A rainfall and PET.

It is also worth noting that forcing Hydrus with CP4A rainfall yields higher soil moisture values regardless of the soil hydraulic parameters used (see Table 3B) or the Feddes' parameters used to estimate the root water uptake of dryland shrubs (see Table 3D).

Hydrus Run (depth meters below ground level)	Site SA (Semi-Arid)	Site A (Arid)
Low (least water resilient) Feddes' Parameters (1.2 mbgl)	6.2	3.6
Low (least water resilient) Feddes' Parameters (3.0 mbgl)	10.7	2.4

https://doi.org/10.5194/egusphere-2025-1154
Preprint. Discussion started: 16 April 2025

Mid Feddes' Parameters (1.2 mbgl)	6.4	8.5
Mid Feddes' Parameters (3.0 mbgl)	10.9	4.7
Default/Upper (most water resilient) Feddes' Parameters (1.2 mbgl)	**10.3**	**15.5**
Default/Upper (most water resilient) Feddes' Parameters (3.0 mbgl)	**20.7**	**9.1**

Table C4 - Relative percentage difference in median depth integrated soil moisture between CP4A and P25 Hydrus runs. Default/Upper (given in bold) refers to default Feddes' parameters that are used for all simulations discussed in the main text, low refers to simulations using the low (least water resilient) Feddes' parameters, and mid refers to simulations using the mid-range Feddes' parameter set. The low, mid, and upper Feddes' parameters are taken from Sela et al (2015). See Appendix 6.1 for more details on each simulation. For all values reported, it is a positive percentage difference between CP4A and P25 soil moisture. Eg CP4A simulates higher soil moisture in all cases.

CP4A + hPET Hydrus Runs	Depth	Site SA	Site A	Site HA	Site HU
	0.2 mbgl	0.12	0.13	0.67	0.09
	0.6 mbgl	0.16	0.28	0.84	0.10
	0.9 mbgl	0.14	0.37	0.86	0.10
	1.2 mbgl	0.19	0.29	0.86	0.10
	1.5 mbgl	0.30	0.19	0.85	0.10
	1.8 mbgl	0.33	0.12	0.84	0.10
	2.1 mbgl	0.35	0.00	0.85	0.10
	2.4 mbgl	0.27	0.00	0.83	0.10
	2.7 mbgl	0.34	0.00	0.80	0.10
	3.0 mbgl	0.20	0.00	0.79	0.10

Table C5 - Kolmogorov–Smirnov (KS) test statistics comparing soil moisture distributions at our hydrological four sites across different depths. Higher KS values indicate greater differences between distributions. All results are statistically significant ($p < 0.05$). Compared to Hydrus simulations driven by CP4A rainfall and PET, those driven by CP4A rainfall and hPET exhibit marginally lower KS values. However, all results remain statistically significant ($p < 0.05$), KS values are Site HU also still exhibit the smallest KS values, suggesting the least divergence.

Default Hydrus Run	Rainfall	PET	Runoff	Infiltration	ET	Evaporation	Transpiration	Drainage
Site SA	5952 (6669)	15750 (16230)	605 (250)	5423 (6398)	6003 (7044)	3611 (5320)	2392 (1724)	286 (23)
Site A	3521 (4289)	19233 (21817)	223 (22)	3297 (4254)	3255 (4283)	2402 (3598)	853 (694)	0 (0)
Site HA	1849 (2394)	17181 (19714)	135 (53)	1713 (2328)	N/A	1574 (2277)	N/A	52 (2)
Site HU	17333 (20003)	13982 (12894)	0 (30)	17300 (19863)	10474 (11418)	4030 (4693)	6445 (6725)	7154 (8638)

Table C6 – Cumulative rainfall, potential evapotranspiration (PET), runoff, infiltration, evapotranspiration (ET), evaporation, transpiration, and drainage from the bottom of the soil profile. All values are given in mm and are the totals over the entire ten-year Hydrus simulations. All results are taken from the default Hydrus run forced with CP4A/P25 rainfall and PET. Those values given in brackets are the P25 Hydrus runs, all others are forced by CP4A.

hPET Hydrus Run	Rainfall	PET	Runoff	Infiltration	ET	Evaporation	Transpiration	Drainage
Site SA	5952 (6669)	15243	566 (246)	5450 (6405)	6052 (7007)	3936 (5382)	2117 (1625)	162 (22)
Site A	3521 (4289)	20223	158 (10)	3330 (4297)	2637 (3789)	2637 (3789)	693 (509)	0 (0)
Site HA	1849 (2394)	18972	94 (51)	1750 (2325)	N/A	1665 (2291)	N/A	36 (1)

https://doi.org/10.5194/egusphere-2025-1154
Preprint. Discussion started: 16 April 2025

Site HU	17333 (20003)	13086	0 (29)	17171 (19810)	10926 (11237)	4188 (4620)	6737 (6617)	6601 (8634)

Table C7 – Cumulative rainfall, potential evapotranspiration (PET), runoff, infiltration, evapotranspiration (ET), evaporation, transpiration, and drainage from the bottom of the soil profile. All values are given in mm and are the totals over the entire ten-year Hydrus simulations. All results are taken from the default Hydrus run forced with CP4A/P25 rainfall and hPET, rather than climate model PET. Those values given in brackets are the P25 rainfall Hydrus runs, all others are forced by CP4A rainfall.

LK Run Type	Runoff	Infiltration	ET	Evaporation	Transpiration	Drainage
Site SA	983 (391)	5043 (6256)	5660 (6928)	3573 (5319)	2087 (1608)	145 (23)
Site A	326 (34)	3192 (4239)	3159 (4273)	2477 (3681)	681 (592)	0 (0)
Site HA	147 (66)	1700 (2314)	N/A	1590 (2273)	N/A	31 (2)
Site HU	4 (43)	17300 (19849)	10485 (11424)	4045 (4709)	6440 (6715)	7145 (8620)
HK Run Type						
Site SA	467 (197)	5564 (6450)	6116 (7075)	3590 (5294)	2525 (1781)	376 (24)
Site A	7 (0)	3512 (4273)	3458 (4308)	2357 (3599)	1100 (709)	0 (0)
Site HA	2 (4)	1846 (2377)	N/A	1641 (2271)	N/A	97 (5)
Site HU	0 (12)	17299 (19880)	10437 (11384)	3999 (4667)	6438 (6717)	7189 (8685)
Lower Feddes Run						
Site SA	611 (254)	5418 (6394)	5807 (6859)	3707 (5433)	2099 (1426)	394 (35)
Site A	176 (23)	3344 (4253)	3314 (4271)	2657 (3734)	657 (537)	4 (3)
Mid Feddes Run						
Site SA	610 (253)	5418 (6394)	5819 (6859)	3697 (5424)	2121 (1435)	382 (31)
Site A	226 (11)	3292 (4261)	3266 (4286)	2514 (3813)	752 (474)	4 (3)
Def Run Type						
Site SA	**605 (250)**	**5423 (6398)**	**6003 (7044)**	**3611 (5320)**	**2392 (1724)**	**286 (23)**
Site A	**223 (22)**	**3297 (4254)**	**3255 (4283)**	**2402 (3598)**	**853 (694)**	**0 (0)**

Table C8 – Cumulative rainfall, potential evapotranspiration (PET), runoff, infiltration, evapotranspiration (ET), evaporation, transpiration, and drainage from the bottom of the soil profile. All values are given in mm and are the totals over the entire ten-year Hydrus simulations. lowK refers to low hydraulic conductivity simulations, and highK is high hydraulic conductivity simulations, while low Feddes' refers to simulations using the low (least water resilient) Feddes' parameters, and mid refers to simulations using the mid-range Feddes' parameter set. The low, mid, and upper (def) Feddes' parameters are taken from Sela et al (2015). See Appendix 6.1 for more details on each simulation. Default (given in bold) values refers to default soil parameters and the upper (default) Feddes' parameters that are used for all simulations discussed in the main text, For All results are taken from the default Hydrus run forced with CP4A/P25 rainfall and PET. Those values given in brackets are the P25 rainfall Hydrus runs, all others are forced by CP4A rainfall.

7. Code Availability

The code used to extract precipitation and all variables needed to compute climate model PET (as well as the code to compute PET) can be found at: https://doi.org/10.6084/m9.figshare.28187072.v2. All other code used to analyse CP4A rainfall/PET data and Hydrus simulations can be provided upon request.

8. Data Availability

CP4A and P25 data is publicly available at the Centre for Environmental Data Analysis Archive under the IMPALA: Improving model processes for African climate. The CP4A/P25 PET datasets for the Horn of Africa can

https://doi.org/10.5194/egusphere-2025-1154
Preprint. Discussion started: 16 April 2025

be downloaded separately from https://doi.org/10.6084/m9.figshare.28187072.v2. Or you can use the provided code to compute PET for another domain. IMERG is publicly available at the NASA Global Precipitation Measurement Mission Data Directory, and the code needed to extract hPET data for any region of interest can be found at: https://github.com/Dagmawi-TA/hPET

9. Author Contribution

GB, KM, EK, MC, and MBS designed this study. GB performed all analysis of climate model data, PET computation, and all Hydrus simulations. EK facilitated access to CP4A data via JASMIN. KM and EK assisted GB in analysis of results. MC assisted in Hydrus parameterisation and model set up. All authors contributed to writing and revising the manuscript.

10. Acknowledgements

This work was funded by the UKRI Natural Research Environment Council under reference NE/S007504/1 with assistance from those funded under the Horizon 2020 DOWN2EARTH project. I would also like to acknowledge the UK Met Office, which provided additional funding and facilitated access to CP4A via JASMIN.

Aspects of the schematic of our Hydrus simulations provided in Figure 2 were created with the use of Artificial Intelligence (DALL·E 3).

11. Competing Interests

The authors declare that they have no conflict of interest.

References

Adloff, M., Singer, M. B., MacLeod, D. A., Michaelides, K., Mehrnegar, N., Hansford, E., Funk, C., and Mitchell, D.: Sustained water storage in Horn of Africa drylands dominated by seasonal rainfall extremes, Geophys. Res. Lett., 49, **https://doi.org/10.1029/2022GL099299**, 2022.

Ageet, S., Fink, A. H., Maranan, M., Diem, J. E., Hartter, J., Ssali, A. L., and Ayabagabo, P.: Validation of satellite rainfall estimates over equatorial East Africa, J. Hydrometeorol., 23, 129–151, https://doi.org/10.1175/JHM-D-21-0145.1, 2022.

Allen, R. G., Pereira, L. S., Raes, D., and Smith, M.: Crop evapotranspiration-Guidelines for computing crop water requirements-FAO Irrigation and Drainage Paper 56, FAO, Rome, 300 pp, 1998.

Apurv, T., Sivapalan, M. and Cai, X.,: Understanding the role of climate characteristics in drought propagation. *Water Resources Research*, *53*(11), pp.9304-9329, **https://doi.org/10.1002/2017WR021445**, 2017.

Archer, L., Hatchard, S., Devitt, L., Neal, J.C., Coxon, G., Bates, P.D., Kendon, E.J. and Savage, J: Future Change in Urban Flooding Using New Convection-Permitting Climate Projections. *Water Resources Research*, *60*(1), **https://doi.org/10.1029/2023WR035533**, 2024.

https://doi.org/10.5194/egusphere-2025-1154
Preprint. Discussion started: 16 April 2025

Ascott, M.J., Christelis, V., Lapworth, D.J., Macdonald, D.M.J., Tindimugaya, C., Iragena, A., Finney, D., Fitzpatrick, R., Marsham, J.H. and Rowell, D.P.: On the application of rainfall projections from a convection-permitting climate model to lumped catchment models. *Journal of Hydrology*, *617*, p.129097, https://doi.org/10.1016/j.jhydrol.2023.129097, 2023.

Ban, N., Schmidli, J., and Schär, C.: Evaluation of the convection-resolving regional climate modeling approach in decade-long simulations, J. Geophys. Res.-Atmos., 119, 7889–7907, **https://doi.org/10.1002/2014JD021478**, 2014.

Batalha, M. S., Barbosa, M. C., Faybishenko, B., and Van Genuchten, M. T.: Effect of temporal averaging of meteorological data on predictions of groundwater recharge, J. Hydrol. Hydromech., 66, 143–152, 2018.

Berthou, S., Rowell, D. P., Kendon, E. J., Roberts, M. J., Stratton, R. A., Crook, J. A., and Wilcox, C.: Improved climatological precipitation characteristics over West Africa at convection-permitting scales, Clim. Dyn., 53, https://doi.org/10.1007/s00382-019-04759-4, 2019.

Boas, T., and Mallants, D.: Episodic extreme rainfall events drive groundwater recharge in arid zone environments of central Australia, J. Hydrol. Reg. Stud., 40, https://doi.org/10.1016/j.ejrh.2022.101005, 2022.

Cheechi, F and Robinson, C. H.: Mortality among populations of southern and central Somalia affected by severe food insecurity and famine during 2010-2012, FAO, Rome, 87pp., 2013

Clark, P., Roberts, N., Lean, H., Ballard, S. P., and Charlton-Perez, C.: Convection-permitting models: A step-change in rainfall forecasting, Meteorol. Appl., 23, 165–181, **https://doi.org/10.1002/met.1538**, 2016.

Cook, P. A., Black, E. C., Verhoef, A., Macdonald, D. M. J., and Sorensen, J. P. R.: Projected increases in potential groundwater recharge and reduced evapotranspiration under future climate conditions in West Africa, J. Hydrol. Reg. Stud., 41, 101076, https://doi.org/10.1016/j.ejrh.2022.101076, 2022.

Corona, C. R., and Ge, S.: Examining subsurface response to an extreme precipitation event using HYDRUS-1D, Vadose Zone J., 21, **https://doi.org/10.1002/vzj2.20189**, 2022.

Crosbie, R. S., McCallum, J. L., Walker, G. R., Francis, H., and Chiew, S.: Modelling climate-change impacts on groundwater recharge in the Murray-Darling Basin, Australia, Hydrogeol. J., 18, 2010.

Cuthbert, M. O., Acworth, R. I., Andersen, M. S., Larsen, J. R., McCallum, A. M., Rau, G. C., and Tellam, J. H.: Understanding and quantifying focused, indirect groundwater recharge from ephemeral streams using water table fluctuations, Water Resour. Res., 52, 827–840, **https://doi.org/10.1002/2015WR017503**, 2016.

Cuthbert, M.O., Gleeson, T., Moosdorf, N., Befus, K.M., Schneider, A., Hartmann, J. and Lehner, B.: Global patterns and dynamics of climate–groundwater interactions. *Nature Climate Change*, *9*(2), https://doi.org/10.1038/s41558-018-0386-4, 2019

Davenport, F., Grace, K., Funk, C., and Shukla, S.: Child health outcomes in sub-Saharan Africa: a comparison of changes in climate and socio-economic factors, Global Environ. Change, 46, 72–87, https://doi.org/10.1016/j.gloenvcha.2017.04.009, 2017.

Davenport, F., Funk, C., and Galu, G.: How will East African maize yields respond to climate change and can agricultural development mitigate this response?, Clim. Change, 147, 491–506, https://doi.org/10.1007/s10584-018-2149-7, 2018.

FAO-SWALIM: Devastating floods overwhelm parts of Somalia, Somalia Flood Update Series: https://www.faoswalim.org/resources/site_files/Devastating%20floods%20Overwhelm%20parts%20of%20Somalia_0.pdf, last access: 19 October 2021.

Feddes, R. A.: Simulation of field water use and crop yield, in: Simulation of Plant Growth and Crop Production, pp. 194–209, 1978.

Finney, D. L., Marsham, J. H., Jackson, L. S., Kendon, E. J., Rowell, D. P., Boorman, P. M., Keane, R. J., Stratton, R. A., and Senior, C. A.: Implications of improved representation of convection for the East Africa water budget using a convection-permitting model, J. Climate, 32, 2109–2129, https://doi.org/10.1175/JCLI-D-18-0387.1, 2019.

Finney, D. L., Marsham, J. H., Rowell, D. P., Kendon, E. J., Tucker, S. O., Stratton, R. A., and Jackson, L. S.: Effects of explicit convection on future projections of mesoscale circulations, rainfall, and rainfall extremes over Eastern Africa, J. Climate, 33, 2701–2718, https://doi.org/10.1175/JCLI-D-19-0328.1, 2020.

https://doi.org/10.5194/egusphere-2025-1154
Preprint. Discussion started: 16 April 2025

Folwell, S.S., Taylor, C.M. and Stratton, R.A.: Contrasting contributions of surface hydrological pathways in convection permitting and parameterised climate simulations over Africa and their feedbacks on the atmosphere. *Climate Dynamics*, *59*(1), pp.633-648., https://doi.org/10.1007/s00382-022-06144-0, 2022.

Funk, C., Shukla, S., Thiaw, W. M., Rowland, J., Hoell, A., McNally, A., Husak, G., Novella, N., Budde, M., Peters-Lidard, C., and Adoum, A.: Recognizing the famine early warning systems network: Over 30 years of drought early warning science advances and partnerships promoting global food security, B. Am. Meteorol. Soc., 100, 1011–1027, https://doi.org/10.1175/BAMS-D-17-0233.1, 2019.

Geißler, K., Heblack, J., Uugulu, S., Wanke, H., and Blaum, N.: Partitioning of water between differently sized shrubs and potential groundwater recharge in a semiarid savanna in Namibia, Front. Plant Sci., 10, 1411, https://doi.org/10.3389/fpls.2019.01411, 2019.

Hengl, T., Miller, M. A., Križan, J., Shepherd, K. D., Sila, A., Kilibarda, M., Antonijević, O., Glušica, L., Dobermann, A., Haefele, S. M., and McGrath, S. P.: African soil properties and nutrients mapped at 30 m spatial resolution using two-scale ensemble machine learning, Sci. Rep., 11, 6130, https://doi.org/10.1038/s41598-021-85639-y, 2021.

Hill, P. G., Stein, T. H., and Cafaro, C.: Convective systems and rainfall in East Africa, Q. J. R. Meteorol. Soc, **https://doi.org/10.1002/qj.4540**, 2023.

Hoffmann, R., Wiederkehr, C., Dimitrova, A., and Hermans, K.: Agricultural livelihoods, adaptation, and environmental migration in sub-Saharan drylands: a meta-analytical review, Environ. Res. Lett., 17, 083003, 2022.

Hsu, H., Lo, M. H., Guillod, B. P., Miralles, D. G., and Kumar, S.: Relation between precipitation location and antecedent/subsequent soil moisture spatial patterns, J. Geophys. Res.-Atmos., 122, 6319–6328, **https://doi.org/10.1002/2016JD026042**, 2017.

Huang, J., Yu, H., Dai, A., Wei, Y. and Kang, L.: Drylands face potential threat under 2 C global warming target. *Nature Climate Change*, *7*(6), pp.417-422, https://doi.org/10.1038/nclimate3275, 2017.

Huffman, G.J., Bolvin, D.T., Braithwaite, D., Hsu, K., Joyce, R., Xie, P. and Yoo, S.H., 2015. NASA global precipitation measurement (GPM) integrated multi-satellite retrievals for GPM (IMERG). *Algorithm theoretical basis document (ATBD) version*, *4*(26), pp.2020-05.

iSDA: The first field-level soil map for Africa: https://www.isda-africa.com/isdasoil/, last access: 20 October 2024

Kendon, E. J., Ban, N., Roberts, N. M., Fowler, H. J., Roberts, M. J., Chan, S. C., Evans, J. P., Fosser, G., and Wilkinson, J. M.: Do convection-permitting regional climate models improve projections of future precipitation change?, Am. Meteorol. Soc., 98, 79–93, https://doi.org/10.1175/BAMS-D-15-0004.1, 2017.

Kendon, E. J., Stratton, R. A., Tucker, S., Marsham, J. H., Berthou, S., Rowell, D. P., and Senior, C. A.: Enhanced future changes in wet and dry extremes over Africa at convection-permitting scale, Nat. Commun., 10, 1794, https://doi.org/10.1038/s41467-019-09776-9, 2019.

Kimutai, J., Barnes, C., Zachariah, M., Philip, S., Kew, S., Pinto, I., Wolski, P., Koren, G., Vecchi, G., Yang, W. and Li, S.: Human-induced climate change increased drought severity in Horn of Africa. https://doi.org/10.1016/j.wace.2025.100745, Weather and Climate Extremes, Vol. 47, https://doi.org/10.1016/j.wace.2025.100745, 2025.

Kipkemoi, I., Michaelides, K., Rosolem, R., and Singer, M. B.: Climatic expression of rainfall on soil moisture dynamics in drylands, Hydrol. Earth Syst. Sci. Discuss., 1–24, https://doi.org/10.5194/hess-2021-48, 2021.

Klein, C., Jackson, L. S., Parker, D. J., Marsham, J. H., Taylor, C. M., Rowell, D. P., Guichard, F., Vischel, T., Famien, A. M., and Diedhiou, A.: Combining CMIP data with a regional convection-permitting model and observations to project extreme rainfall under climate change, Environ. Res. Lett., 16, 2021.

Kouadio, K., Bastin, S., Konare, A., and Ajayi, V. O.: Does convection-permitting simulate better rainfall distribution and extreme over Guinean coast and surroundings?, Clim. Dyn., 55, 153–174, https://doi.org/10.1007/s00382-018-4308-y, 2020.

Leterme, B., Mallants, D., and Jacques, D.: Estimation of future groundwater recharge using climatic analogues and Hydrus-1D, Hydrol. Earth Syst. Sci. Discuss., 9, 2012.

https://doi.org/10.5194/egusphere-2025-1154
Preprint. Discussion started: 16 April 2025

Lobell, D. B., Bänziger, M., Magorokosho, C., and Vivek, B.: Nonlinear heat effects on African maize as evidenced by historical yield trials, Nat. Clim. Change, 1, 42–45, https://doi.org/10.1038/nclimate1043, 2011.

Luu, L. N., Vautard, R., Yiou, P., and Soubeyroux, J. M.: Evaluation of convection-permitting extreme precipitation simulations for the south of France, Earth Syst. Dynam., 13, 687–702, https://doi.org/10.5194/esd-13-687-2022, 2022.

Lyon, B. and Vigaud, N.: Unraveling East Africa's climate paradox. *Climate extremes: Patterns and mechanisms*, **https://doi.org/10.1002/9781119068020.ch16**, 2017.

Lyon, B.: Seasonal drought in the Greater Horn of Africa and its recent increase during the March–May long rains. *Journal of Climate*, *27*(21), https://doi.org/10.1175/JCLI-D-13-00459.1, 2014.

Maeght, J. L., Rewald, B., and Pierret, A.: How to study deep roots—and why it matters, Front. Plant Sci., 4, 299, https://doi.org/10.3389/fpls.2013.00299, 2013.

McKenna, O. P., and Sala, O. E.: Groundwater recharge in desert playas: current rates and future effects of climate change, Environ. Res. Lett., 13, 014025, 2017.

Mirzabaev, A., et al.: Desertification, in: Climate Change and Land: an IPCC special report on climate change, desertification, land degradation, sustainable land management, food security, and greenhouse gas fluxes in terrestrial ecosystems, IPCC, 2019.

Muñoz Sabater, J.: ERA5-Land hourly data from 1950 to present, Copernicus Climate Change Service (C3S) Climate Data Store (CDS), https://doi.org/10.24381/cds.e2161bac, 2019.

Nazarieh, F., Ansari, H., Ziaei, A. N., Izady, A., Davari, K., and Brunner, P.: Spatial and temporal dynamics of deep percolation, lag time and recharge in an irrigated semi-arid region, Hydrogeol. J., 26, 2507–2520, 2018.

Nicholson, S. E.: Dryland Climatology, Cambridge University Press, Cambridge, 2011.

Osborn, H. B.: Timing and duration of high rainfall rates in the southwestern United States, Water Resour. Res., 19, 1036–1042, 1983.

Porporato, A., D'Odorico, P., Laio, F., Ridolfi, L., and Rodriguez-Iturbe, I.: Ecohydrology of water-controlled ecosystems, Adv. Water Resour., 25, 1335–1348, https://doi.org/10.1016/S0309-1708(02)00058-1, 2002.

Prein, A. F., Gobiet, A., Suklitsch, M., Truhetz, H., Awan, N. K., Keuler, K., and Georgievski, G.: Added value of convection-permitting seasonal simulations, Clim. Dyn., 41, 2655–2677, https://doi.org/10.1007/s00382-013-1744-6, 2013.

Prein, A. F., Langhans, W., Fosser, G., Ferrone, A., Ban, N., Goergen, K., Keller, M., Tölle, M., Gutjahr, O., Feser, F., and Brisson, E.: A review on regional convection-permitting climate modeling: Demonstrations, prospects, and challenges, Rev. Geophys., 53, 323–361, **https://doi.org/10.1002/2014RG000475**, 2015.

Quichimbo, E. A., Singer, M. B., and Cuthbert, M. O.: Characterising groundwater–surface water interactions in idealised ephemeral stream systems, Hydrol. Process., 34, 3792–3806, **https://doi.org/10.1002/hyp.13847**, 2021.

Quichimbo, E. A., Singer, M. B., Michaelides, K., Rosolem, R., MacLeod, D. A., Asfaw, D. T., and Cuthbert, M. O.: Assessing the sensitivity of modelled water partitioning to global precipitation datasets in a data-scarce dryland region, Hydrol. Process., 37, e15047, **https://doi.org/10.1002/hyp.15047**, 2023.

Razack, M., Jalludin, M., and Houmed-Gaba, A.: Simulation of climate change impact on a coastal aquifer under arid climate. The Tadjourah Aquifer (Republic of Djibouti, Horn of Africa), **https://doi.org/10.3390/w11112347**, 2019.

Reynolds, J. F., Smith, D. M. S., Lambin, E. F., Turner, B. L., Mortimore, M., Batterbury, S. P., Downing, T. E., Dowlatabadi, H., Fernández, R. J., Herrick, J. E., and Huber-Sannwald, E.: Global desertification: building a science for dryland development, Science, 316, 847–851, 2007.

Reynolds, R. W., Smith, T. M., Liu, C., Chelton, D. B., Casey, K. S., and Schlax, M. G.: Daily high-resolution-blended analyses for sea surface temperature, J. Clim., 20, 5473–5496, https://doi.org/10.1175/2007JCLI1824.1, 2007.

Richards, L. A.: Capillary conduction of liquids through porous mediums, Phys., 1, 318–333, 1931.

https://doi.org/10.5194/egusphere-2025-1154
Preprint. Discussion started: 16 April 2025

Rios Gaona, M.F., Michaelides, K. and Singer, M.B.: STORM v. 2: A simple, stochastic rainfall model for exploring the impacts of climate and climate change at and near the land surface in gauged watersheds. *Geoscientific Model Development*, *17*(13), pp.5387-5412, https://doi.org/10.5194/gmd-17-5387-2024, 2024.

Rodriguez, P., Giménez, R., Nosetto, M. D., Jobbágy, E. G., and Magliano, P. N.: Changes in water fluxes partition related to the replacement of native dry forests by crops in the Dry Chaco, J. Arid Environ., 183, 104281, https://doi.org/10.1016/j.jaridenv.2020.104281, 2020.

Scanlon, B. R., Keese, K. E., Flint, A. L., Flint, L. E., Gaye, C. B., Edmunds, W. M., and Simmers, I.: Global synthesis of groundwater recharge in semiarid and arid regions, Hydrol. Process., 20, 3335–3370, **https://doi.org/10.1002/hyp.6335**, 2006.

Schimel, D. S.: Drylands in the earth system, Science, 327, 418–419, 2010.

Schoener, G., and Stone, M. C.: Impact of antecedent soil moisture on runoff from a semiarid catchment, J. Hydrol., 569, 627–636, https://doi.org/10.1016/j.jhydrol.2018.12.025, 2019.

Schoener, G.: Soil Moisture Dependent Runoff in a Dryland Region: An Investigation of the Role of Antecedent Conditions, Monitoring, and Modeling Strategies, PhD Thesis, University of New Mexico. 2021.

Schwarzwald, K., and Seager, R.: Revisiting the 'East African Paradox': CMIP6 models also fail to simulate observed drying trends in the Horn of Africa Long Rains, Copernicus Meetings, No. EGU24-4687, 2024.

Schwarzwald, K., Goddard, L., Seager, R., Ting, M., and Marvel, K.: Understanding CMIP6 biases in the representation of the Greater Horn of Africa long and short rains, Clim. Dyn., 61, 1229–1255, https://doi.org/10.1007/s00382-022-06622-5, 2023.

Seddon, D., Kashaigili, J. J., Taylor, R. G., Cuthbert, M. O., Mwihumbo, C., and MacDonald, A. M.: Focused groundwater recharge in a tropical dryland: Empirical evidence from central, semi-arid Tanzania, J. Hydrol. Reg. Stud., 37, https://doi.org/10.1016/j.ejrh.2021.100919, 2021.

Sela, S., Svoray, T., and Assouline, S.: The effect of soil surface sealing on vegetation water uptake along a dry climatic gradient, Water Resour. Res., 51, 7452–7466, **https://doi.org/10.1002/2015WR017109**, 2015.

Shadwell, E., and February, E.: Effects of groundwater abstraction on two keystone tree species in an arid savanna national park, PeerJ, 5, 2017.

Šimunek, J., Van Genuchten, M.T. and Šejna, M., 2012. HYDRUS: Model use, calibration, and validation. *Transactions of the ASABE*, *55*(4), pp.1263-1274.

Singer, M. B., and Michaelides, K.: Deciphering the expression of climate change within the Lower Colorado River basin by stochastic simulation of convective rainfall, Environ. Res. Lett., 12, 2017.

Singer, M. B., Michaelides, K., and Hobley, D. E. J.: STORM 1.0: A simple, flexible, and parsimonious stochastic rainfall generator for simulating climate and climate change, Geosci. Model Dev., 11, 3713–3726, https://doi.org/10.5194/gmd-11-3713-2018, 2018.

Singer, M.B., Asfaw, D.T., Rosolem, R., Cuthbert, M.O., Miralles, D.G., MacLeod, D., Quichimbo, E.A. and Michaelides, K.: Hourly potential evapotranspiration at 0.1 resolution for the global land surface from 1981-present. *Scientific Data*, *8*(1), https://doi.org/10.1038/s41597-021-01003-9, 2021.

Stephens, G. L., L'Ecuyer, T., Forbes, R., Gettelmen, A., Golaz, J. C., Bodas-Salcedo, A., Suzuki, K., Gabriel, P., and Haynes, J.: Dreary state of precipitation in global models, J. Geophys. Res.-Atmos., 115, D24211, **https://doi.org/10.1029/2010JD014532**, 2010.

Stone, E. L., and Kalisz, P. J.: On the maximum extent of tree roots, For. Ecol. Manage., 46, 59–102, 1991.

Stratton, R. A., and Stirling, A. J.: Improving the diurnal cycle of convection in GCMs, Q. J. R. Meteorol. Soc., 138, 1121–1134, **https://doi.org/10.1002/qj.991**, 2012.

Stratton, R. A., Senior, C. A., Vosper, S. B., Folwell, S. S., Boutle, I. A., Earnshaw, P. D., Kendon, E., Lock, A. P., Malcolm, A., Manners, J., and Morcrette, C. J.: A Pan-African convection-permitting regional climate simulation with the Met Office Unified Model: CP4-Africa, J. Clim., 31, 3485–3508, https://doi.org/10.1175/JCLI-D-17-0503.1,2018.

https://doi.org/10.5194/egusphere-2025-1154
Preprint. Discussion started: 16 April 2025

Stringer, L. C., Dyer, J. C., Reed, M. S., Dougill, A. J., Twyman, C., and Mkwambisi, D.: Adaptations to climate change, drought and desertification: local insights to enhance policy in southern Africa, Environ. Sci. Policy, 12, 748–765, https://doi.org/10.1016/j.envsci.2009.04.002, 2009.

Taylor, C. M., de Jeu, R. A., Guichard, F., Harris, P. P., and Dorigo, W. A.: Afternoon rain more likely over drier soils, Nature, 489, 423–426, https://doi.org/10.1038/nature11377, 2012.

Taylor, C. M., Gounou, A., Guichard, F., Harris, P. P., Ellis, R. J., Couvreux, F., and De Kauwe, M.: Frequency of Sahelian storm initiation enhanced over mesoscale soil-moisture patterns, Nat. Geosci., 4, 430–433, https://doi.org/10.1038/ngeo1173, 2011.

Taylor, R. G., Todd, M. C., Kongola, L., Maurice, L., Nahozya, E., Sanga, H., and MacDonald, A. M.: Evidence of the dependence of groundwater resources on extreme rainfall in East Africa, Nat. Clim. Change, 3, 374–378, https://doi.org/10.1038/nclimate1731, 2013.

Tugwell-Wootton, T., Skrzypek, G., Dogramaci, S., McCallum, J., and Grierson, P. F.: Soil moisture evaporative losses in response to wet-dry cycles in a semiarid climate, J. Hydrol., 590, 125533, https://doi.org/10.1016/j.jhydrol.2020.125533, 2020.

Van Genuchten, M. T.: A closed-form equation for predicting the hydraulic conductivity of unsaturated soils, Soil Sci. Soc. Am. J., 44, 892–898, 1980.

Vermote, E.: NOAA Climate Data Record (CDR) of AVHRR Leaf Area Index (LAI) and Fraction of Absorbed Photosynthetically Active Radiation (FAPAR), Version 5, NOAA National Centers for Environmental Information, 2019.

Vicente-Serrano, S. M., Miralles, D. G., Domínguez-Castro, F., Azorin-Molina, C., El Kenawy, A., McVicar, T. R., Tomás-Burguera, M., Beguería, S., Maneta, M., and Peña-Gallardo, M.: Global assessment of the standardized evapotranspiration deficit index (SEDI) for drought analysis and monitoring, J. Clim., 31, 5371–5393, https://doi.org/10.1175/JCLI-D-17-0775.1, 2018.

Wainwright, C.M., Marsham, J.H., Keane, R.J., Rowell, D.P., Finney, D.L., Black, E. and Allan, R.P., 2019. 'Eastern African Paradox' rainfall decline due to shorter not less intense Long Rains. *npj Climate and Atmospheric Science*, *2*(1), https://doi.org/10.1038/s41612-019-0091-7, 2019.

Wainwright, C. M., Finney, D. L., Kilavi, M., Black, E., and Marsham, J. H.: Extreme rainfall in East Africa, October 2019–January 2020 and context under future climate change, Weather, 76, 26–31, **https://doi.org/10.1002/wea.3824**, 2021.

Walters, D., Boutle, I., Brooks, M., Melvin, T., Stratton, R., Vosper, S., Wells, H., Williams, K., Wood, N., Allen, T. and Bushell, A.: The Met Office unified model global atmosphere 6.0/6.1 and JULES global land 6.0/6.1 configurations. *Geoscientific Model Development*, *10*(4), pp.1487-1520, https://doi.org/10.5194/gmd-10-1487-2017, 2017.

Watson, A.: The use of environmental isotopes, soil water measurements and soil water modelling to understand tree water use of an Acacia mearnsii (Black Wattle) stand in KwaZulu-Natal, MSc Thesis, University of KwaZulu-Natal, 135 pp., 2015.

Wesseling, J. G., Elbers, J. A., Kabat, P., and Van den Broek, B. J.: SWATRE: instructions for input, Internal Note, Winand Staring Centre, Wageningen, the Netherlands, p. 700, 1991.

Xia, Y. Q., and Shao, M. A.: The process modeling of soil water carrying capacity for vegetation in small watershed within the wind-water crisscrossed erosion zone on the Loess Plateau, Institute of Geographical Sciences and Natural Resources Research, Chinese Academy of Sciences, 2008.

Zarate, E., Hobley, D., MacDonald, A. M., Swift, R. T., Chambers, J., Kashaigili, J. J., Mutayoba, E., Taylor, R. G., and Cuthbert, M. O.: The role of superficial geology in controlling groundwater recharge in the weathered crystalline basement of semi-arid Tanzania, J. Hydrol. Reg. Stud., 36, 100833, https://doi.org/10.1016/j.ejrh.2021.100833, 2021.

Zhang, Y. K., and Schilling, K. E.: Effects of land cover on water table, soil moisture, evapotranspiration, and groundwater recharge: a field observation and analysis, J. Hydrol., 319, 328–338, https://doi.org/10.1016/j.jhydrol.2005.06.044, 2006.

Zhou, S., Williams, A. P., Lintner, B. R., Berg, A. M., Zhang, Y., Keenan, T. F., Cook, B. I., Hagemann, S. I., Seneviratne, S. I., and Gentine, P.: Soil moisture–atmosphere feedbacks mitigate declining water availability in drylands, Nat. Clim. Change, 11, 38–44, https://doi.org/10.1038/s41558-020-00945-z, 2021.

Zinyengere, N., Mhizha, T., Mashonjowa, E., Chipindu, B., Geerts, S., and Raes, D.: Using seasonal climate forecasts to improve maize production decision support in Zimbabwe, Agric. For. Meteorol., 151, 1792–1799, https://doi.org/10.1016/j.agrformet.2011.07.015, 2011.

https://doi.org/10.5194/egusphere-2025-1154
Preprint. Discussion started: 16 April 2025

995 Zomer, R., Trabucco, A., van Straaten, O., and Bossio, D.: Carbon, land and water: A global analysis of the hydrologic dimensions of climate change mitigation through afforestation/reforestation, IWMI, Vol. 101, 2007.